2-19-2018

Microfluidic Technology and Application in Urinal Analysis

Jiwen Xiang
Louisiana State University and Agricultural and Mechanical College

MICROFLUIDIC TECHNOLOGY AND APPLICATION IN URINALYSIS

A Dissertation

Submitted to the Graduate Faculty of the
Louisiana State University and
Agricultural and Mechanical College
in partial fulfillment of the
requirements for the degree of
Doctor of Philosophy

in

The Department of Mechanical Engineering

by
Jiwen Xiang
B.S., Central South University, China, 2010
M.S., Central South University, China, 2013
May 2018

ACKNOWLEDGEMENTS

First and foremost, I would like to thank my major advisor, Dr. Wanjun Wang, for all his contributions of time, ideas, and funding to make my Ph.D. experience productive and stimulating. The joy and enthusiasm he has for life and research was contagious and motivational for me, especially during tough times in the Ph.D. pursuit.

I also want to thank my committee members, Dr. Jin-Woo Choi, Dr. Shengmin Guo, Dr. Manas Gartia, and the Dean's Representative, Dr. Graça Vicente, for their professional advice.

The members of the Wang's group have contributed immensely to my personal and professional time at Louisiana State University. Special thanks should be given to group members Ziliang Cai and Yong Zhang for their insightful suggestions and unconditional assistance throughout the project.

Finally, my grateful appreciation goes to my parents, my wife and my son. Without your firm support and love, I never would have made it through this process or any of the tough times in my life. Thank you.

TABLE OF CONTENTS

LIST OF FIGURES

ABSTRACT

Microfluidic technology offers numerous advantages in minimizing and integrating the traditional assays. However, the lack of efficient control components of the microfluidic systems has been hindering the widely commercialization of the technology. The research work in this dissertation focused on the development of effective control components for microfluidic applications.

A linear peristaltic pump was firstly designed, fabricated, and tested for conventional microfluidics by synchronously compressing the microfluidic channel with a miniature cam-follower system in Chapter 2. The miniature cam-follower system and microfluidic chip was prototyped using three-dimensional (3D) printing technology and soft lithography technology. Results from experimental test showed that the pump is self-priming and tolerant of bubbles. The pumping flowrate and back pressure could be controlled by changing the driving speed of the motor.

Then a novel pinch-type valving system that can be used to realize both normally closed and normally open valves for centrifugal microfluidics was demonstrated in Chapter 3. A sliding wedge was actuated by centrifugal force to drive the valves. Experimental test and theoretical predication showed that the burst frequency of the valves could be tuned by changing the physical parameters of the valving system. In Chapter 4, the pinch type valving system was then further improved for better integration of multiple valves in limited space to realize sequential control of microfluidics. A valve chip with grooves on the surface was used

to drive multiple valves. A flow switch which is capable of working at low rotation frequency and constant rotation direction is realized.

Finally, the microfluidic platform was utilized for automatic urinalysis for the application at point of care (POC) to eliminate the difficulties in control of sample distribution and read-out time in manually conducted colorimetric urinalysis. 3D printed prototype of the microfluidic chip was used to test the proposed system. Commercial urinalysis strips was integrated with the microfluidic system for detecting glucose, specific gravity, PH, and protein from simulated urine sample. The color change of the pads was recorded using smartphone camera and analyzed to quantify the interested parameters.

CHAPTER 1. INTRODUCTION

Microfluidics is the science and technology of microsystems with ability to manipulate liquid flows at the sub-millimeter scale within micro channels or other microstructures [1]. The liquid samples are often transported though the micro channels and chambers with designed time sequence and sample volume to precisely control the reaction assays in miniaturized scales. Some properties coming with the miniaturization, such as drastically decreased demand of reaction time and consumption of expensive chemical reagents, precise control of reagent flow and particles, enhancement of reliability and consistency, high resolution and sensitivity, easier parallelization and automation, have been attractive in replacing the traditional macroscale lab assays [1,2]. Additionally, the ability of microfluidics to realize large array of assays in a small and disposable chip with low cost provides great potential for low-cost point-of-care (POC) usage.

1.1 Application of microfluidic system

Microfluidics system, also being referred to as miniaturized total analysis systems (mTAS) or lab-on-a-chip (LoC), has been investigated in a wide range of areas for improving the biomedical and chemical assays. In biomedical field, microfluidics was used for testing the efficacy of the new discoveries in drug screening [3], disease diagnosis [4–6], DNA analysis [7,8], cell and particle separation [9–11], cell cytometry [12], cell manipulation [13,14] and so on. Gene sequencing are one of the most promising field for the commercialization of microfluidic technology. Microfluidics offered higher throughput, sensitivity and resolution than conventional analytical methods, and thus been considered

attractive for automating and expediting the processing in genomics of next-generation sequencing technology after the completion of the human genome project in 2003 [1]. Besides the gene sequencing, POC diagnostics is another area that greatly benefits form the development of microfluidics technology. Microfluidics has been the most likely technological driver for rapid and real-time analysis of disease markers from a small volume of bodily fluids. By integrating sample manipulation, reaction and detection units into a small disposable system, microfluidics enables the realization of disease diagnosis in resource-poor settings with reliable results and simple manual operations. Many ventures have emerged to commercialize microfluidic technologies for POC diagnosing diseases like diabetes, HIV/AIDS, bacterial infections, malaria and so on [15].

For chemistry, microfluidics showed the ability in boosting traditional reactions in various aspects. Due to the scale-dependent processes of heat and mass transfer, the large ratios of surface area to volume, high throughput, superior reaction controllability, and safer operational environment, microfluidics provides outstanding reactors for chemical synthesis [16], fuel cells [17], photocatalysis [18] and many other applications. This technology is especially attractive for green chemistry which aims to decrease the required energy in chemical synthesis, increase the throughput in unit area, decrease reagent consumption and use less hazardous chemicals [16].

1.2 Fabrication of microfluidic chip

In the early stage of microfluidic technology development, microfluidic chips were fabricated based on the mature fabrication technology for microelectronics. The channels and

chambers were directly etched on silicon or glass to construct the microfluidic network. The mechanical stability of silicon and glass are useful to guarantee the stability of geometry of the microstructures in the microfluidic chip, which is especially significant when the dimension of the structures go to nanoscale or lower. However, microfluidic systems based on silicon and glass quickly showed their limitation in usages involving high voltage or applications requiring the device to be transparent in visible and ultraviolet light [1]. Besides, the bonding step for silicon or glass microfluidic devices is generally expensive [19]. Additionally, it is more difficult to fabricate the pumps and valves for microfluidics based on the rigid silicon and glass compared with the elastomer based ones [1].

Later, high precision computer- numerically controlled (CNC) machines were used for fabricating microfluidic chips. Either the fluidic network or the master mould for the network could be engraved on metal or plastic sheets. Resolutions of the order of 50–100 μm could be directly realized using conventional milling techniques [19]. Various kinds of plastics with different properties could be chosen to fabricate microfluidics for different applications. These plastics are generally cheap and easy to be machined. Disadvantages, such as complex tool alignment, expensive for small scale production, have been slowing down the widely application of this technology in fabrication of microfluidic system.

The soft lithography technology enabled the fast prototyping of microfluidics and has been the most popular method to construct microfluidic chip in lab stage since then [20]. PDMS, an optically transparent and biocompatible elastomer, could be directly molded against the masters to form complex microfluidic structures with low cost. The dimension of

the molded microfluidic structures can go to nanoscale and structures on planar, curved, and flexible can all be fabricated. Another advantage of PDMS microfluidic system is their easily bonding to glass slide after being processed by oxygen plasma or sealing with other transparent plastic slide after some simple processes [21]. Besides, PDMS structures could be easily deformed, thus made it possible to integrate valves and pumps, which functioned by deforming the microfluidic channels, with the microfluidic chip [22]. Even though coming with these advantages, PDMS casting is still not the final solution to fabricate microfluidics because PDMS swells in most solvents and the porous structure of cured PDMS weakens its airtightness [23].

Recently, to fabricate microfluidic systems using three-dimensional (3D) printing technology has gained significant attention due its advantages in fast prototyping microfluidic with a wide range of alternative materials. It is especially useful for fabricating these microfluidic systems with complicated spatial structures which are otherwise hard to be fabricated using the traditional manufacturing process, such as photolithography, CNC machining or soft lithography technology.

3D printing is a fabrication process which translates 3D computer designs into physical 3D models by additive layer-by-layer patterning. Numerous types of 3D printing technologies have been applied to fabricate microfluidics. Stereolithography (SL), multi jet modeling (MJM) and fused deposition modelling (FDM) are most commonly used for microfluidic device fabrication [24]. 3D-printing technologies have the advantages in fast production of small batches of products. But the resolution of current 3D printing technology generally

stays around hundreds of microns, which is hard to compete with other fabrication methods, such as photolithography. In addition, difficulties such as removing the support material for suspended structures still need to be overcome for fabricating the tiny microchannel and chambers.

1.3 Control of microfluidic system

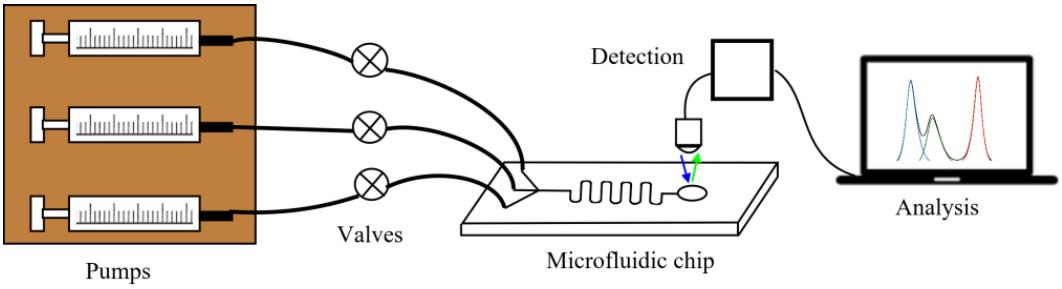

Figure 1.1 Typical setup of a microfluidic system

The core functionality of microfluidic system is to manipulate microscopic volumes of fluid samples. All the manipulations of the samples happen in the microfluidic chip. The chambers and reservoirs in the microfluidic chip provided locations for holding the sample and reactions of the samples. These chambers and reservoirs are connected by microchannels, so that the liquid samples could be transported from one location to another. Conventional microfluidic chips were generally fabricated on a flat substrate, such as glass slide. Figure 1.1 shows a typical setup of conventional microfluidic system. Pumps and valves are two most important components for realizing sample manipulations within the microfluidic chip. Pumping is used for transporting the sample to pass through the microchannel in the microfluidic chip. Valves are required for regulating the sample flow in the microfluidic chip,

so that the liquid flow could be blocked at designed locations of the microfluidic system for designed time period and released when necessary.

Generally, external pumps are used for delivering the sample through the microchannel of conventional microfluidic chip. Pumps are connected to the microfluidic chip using tubes and connectors. Each of the sample flow paths normally requires a separated pump. Various types of commercial pumps for microfluidic system could be found in the market, such as syringe pump, peristaltic pump and so on. External pump is an essential component in a conventional microfluidic system. The need for external pumps increased the cost and complexity of the system. In order to eliminate the requirement for expensive and bulky pump for delivering each sample through the microfluidic channel, centrifugal platform was proposed for pump-free microfluidic system. Microfluidic systems based on centrifugal platform are called centrifugal microfluidics or Lab-on-CD. In centrifugal microfluidics, several forces are exerted on fluid sample in the microchannel because of the rotation of the platform. These forces include: the centrifugal fugal force (Fc), the Coriolis force (F_{co}) and the Euler force (F_E), as shown in Figure 1.2.

When the microfluidic disc was driven to rotate, a free liquid droplet with mass *m* in the microfluidic channel is pumped to flow to the edge of the rotating platform under the centrifugal force. Centrifugal force can be calculated by the following equation:

$$F_c = -m\vec{\omega} \times \left(\vec{\omega} \times \vec{r}\right), \qquad (1\text{-}1)$$

where $\vec{r}$ is the position vector of the fluid droplet on the rotational platform, $\vec{\omega}$ is the angular velocity of the platform.

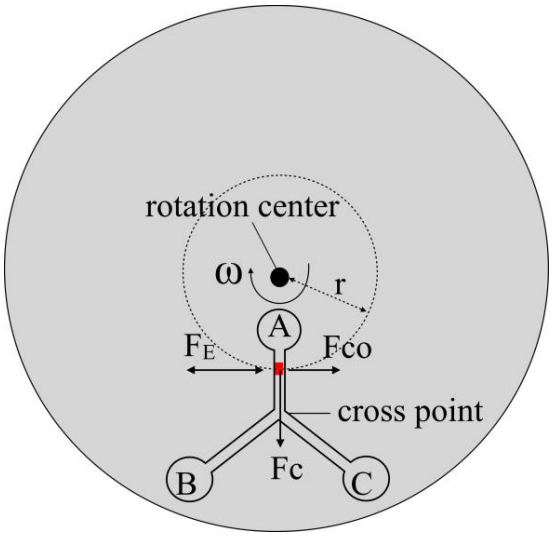

Figure 1.2 Inertia forces acting on centrifugal microfluidics

Because of the motion of the droplets relative to the rotating platform (the reference frame), a Coriolis force is also exerted on the droplet. When the liquid drop flows through the channel, Coriolis force on the liquid drop is perpendicular to both the angular speed and the relative velocity of the droplet with respective to the rotational platform. Coriolis force can be calculated as,

$$F_{CO} = -2m\vec{\omega} \times \frac{d}{dt}\vec{r} \quad . \qquad (1\text{-}2)$$

Under actuation of the centrifugal force, fluids in the channel will always flow outside from the rotation center, so the direction of Coriolis force is determined by the angular speed of the platform as shown in Equation (1-2). Thus Coriolis could be used to control the flow direction at the cross point as shown in Figure 1.2. When the platform is rotating in the clockwise direction, the Coriolis force on the fluidic drop will act toward to the right-side, so fluidic from Chamber A will move into Chamber C. On the other hand, when the rotating direction is reversed to counter-clockwise direction, fluid is driven to move into chamber B.

Beside the Coriolis force, the moving direction of the liquid drop will be affected by another inertia force, the Euler force, when the platform is in the accelerating or decelerating stage. The Euler force (F_E) can be calculated using Equation (3) as,

$$F_E = -m\frac{d}{dt}\vec{\omega} \times \vec{r} \qquad (1\text{-}3)$$

From Equation (1-3), the direction of Euler force is determined by the direction of the acceleration. So when the platform accelerates in clockwise direction or decelerates in counter-clockwise direction, Euler force will act toward to the right-side and will pull the fluid drop to move into channel C. When the platform accelerates in counter-clockwise direction or decelerates in clockwise direction, Euler force will act toward to the left-side and will pull the fluid drop to move into channel B.

Centrifugal force has long been utilized to transfer samples through different steps in chemical and biological assays. In late 1960s, N. Anderson from Oak Ridge National Labs proposed a centrifugal analyser for clinical chemistry assays [25,26]. In their design, the centrifugal analyser incorporated a rotating disc with multiple reservoirs. The reservoirs were connected with fluidic channels to form a fluidic system. Physical barriers were designed for these reservoirs to keep the reagents separated when loading the samples. When the disc rotates, centrifugal force drives the fluids in the reservoirs to pass the physical barriers and move toward the edge of the disc to realize the designed reaction series or detection.

In the past decades, work has been done continuingly to shrink the size of centrifugal analyser for better portability, reagent saving, cost effective and complete integration of sample processing. In 1998, M. Madou et al. introduced the microfabrication techniques into

centrifugal analyser to form the centrifugal microfluidic system [27]. The basic theories and designs of centrifugal microfluidic technology were gradually developed. Different operation units, such as the valving, metering, sample storing, mixing, switching have been developed for various assays on centrifugal microfluidic platform [28]. In recent years, centrifugal microfluidic technology has evolved to become a very attractive option in realizing the high-throughput sample-to-answer process automatically with fewer manual operations.

1.4 Status of the microfluidic technology

The origination of microfluidic devices can be traced back to the work on a chip-based gas chromatograph in 1939 [29]. In the early 1990s, studies by Manz and coworkers initiated the research of microfluidic systems as they are understood today [30]. In the past decades, tremendous researches have been conducted in exploring the full potential of microfluidics. The microfluidic systems technologies have the potentials to get a big commercial success in human genome project and point of care (POC) detection. However, these potentials still have not yet become reality until today. Researchers are still looking for a 'killer application' to enhance its appeal to the market place.

It is difficult to identify a single reason for the gap between the optimism expectation and the reality of marketization of microfluidic technology. Beside the absence of 'killer applications, one of the most possible reasons is the lack of reliable microfluidic components, i.e., micropumps and microvalves, to make this technology easy to be accepted by the market. When the cost of setting up a microfluidic system to manipulate sample is too high or the

operation of the microfluidic system is too complex, people may still tend to keep the conventional approaches for conducting assays. Even though much effort has been put to the development of the microfluidic control components, they are still in highly desired to be push forward [31].

1.5 Scope of the research

The research work presented will focus on the development of the control components of microfluidics, i.e., the pumps and valves for regulating the liquid sample in the microfluidic chip.

For conventional slide based microfluidics, a peristaltic pump was developed in Chapter 2. A linear peristaltic pump has been designed, fabricated, and tested for microfluidic applications. The operation of the pump is based on synchronously compressing the microfluidic channel with a miniature cam-follower system. The flexible microfluidic channel was fabricated with elastomer polydimethylsiloxane (PDMS) using soft lithography. The miniature cam-follower system was fabricated using three-dimensional (3D) printing technology.

For centrifugal microfluidics, the control focused on the valving of the microfluidic flow. Valves actuated by centrifugal force were studied in Chapter 3 and Chapter 4. A novel pinch-type valving technology, which can be used to realize both normally closed and normally open valves for fluidic control on centrifugal microfluidic platform, was presented in Chapter 3. A sliding wedge with inclined surface planes was used to transduce the actuation of the centrifugal force from radial direction to the perpendicular direction of the

microfluidic disc. The function of the valves has been demonstrated experimentally using a PDMS microfluidic system.

In Chapter 4, the valving system was further improved for application in sequential control of microfluidics by introducing a grooved valve chip to drive spring ball plungers mounted under the microfluidic chip to close the microfluidic channel. By mechanically programing the location of the grooves on the valve chip, the switch sequence of the valves could be programmed. The performance of the valve system was tested using a 3D printed microfluidic chip.

Finally, colorimetric urinalysis based on the centrifugal microfluidic platform was conducted. Centrifugal microfluidic chip was introduced for controlling the distribution of urine sample in designed volume and time sequence. The mechanical valving system was used to regulate the time sequence of sample release. Microfluidic chip prototype was fabricated using 3D printing technology and used to test the proposed system.

CHAPTER 2. A MICRO-CAM ACTUATED LINEAR PERISTALTIC PUMP FOR CONVENTIONAL MICROFLUIDICS

2.1 Introduction

Microfluidic technology has remarkably promoted the development of point-of-care (POC) testing which is capable of providing rapid and inexpensive onsite clinical diagnosis [15]. One challenge for the POC applications of microfluidic technologies is the need for compact and efficient pumps to deliver a microscopic amount of fluidic samples through the microchannels. Various kinds of pumps have been investigated for microfluidic systems, such as syringe pump [32,33], electrokinetic pump [34,35], acoustic pump [36,37], peristaltic pump [38–40]. Syringe pump is highly efficient and stable, but it is bulky and expensive, thus difficult to be integrated with portable microfluidic systems. Electrokinetic pump has simple design and can work with high backpressures, but it requires supply of high voltage (kilovolts). Acoustic pumps could precisely manipulate fluids but they are limited in use because of the low pumping flow rate and low allowable back -pressure.

Peristaltic pump works by compressing the flexible fluidic channel to displace the liquid in the channel forward [39–41]. Even though suffering from problems like mechanical wear, it is still a good option for microfluidics because of its key advantages. Due to the mechanism of flow delivery, the external actuating components of peristaltic pump have no contact with the fluids in the channel, so the sample contamination caused by the pumps could be minimized. Besides, peristaltic pump could be used to generate rapid bi-directional flow and circulating flow in microfluidic channels, which is otherwise difficult to be realized using other pumping mechanisms. Integration of peristaltic pumps into microfluidics requires

minimized actuation mechanisms for the compression. Pneumatic actuation is the most common actuation mechanism in microfluidics [22,42,43]. This kind of pump is composed of at least three pneumatic valves. The valves close the channel synchronously to transport the fluid through the channel. However, high-pressure gas source and solenoid valves are required to actuate and control the turn on/off the pneumatic valves. The pneumatic actuation should be carefully timed by peripheral circuits to make the valves work in a synchronized pattern to pump fluids. Besides, when the microfluidic chip need to be replaced, the tubes connecting the gas source and the pneumatic control channel in the chip should be reconnected, which is time consuming and difficult to be implemented by nonprofessional users.

Other actuation techniques have been investigated to replace the pneumatic actuation. Discrete permanent magnet pair with one of the magnet fixed on deformable channel and another rotating with a motor shaft holds the potential of simplifying the fabrication and operation of the peristaltic pump [44,45]. When the shaft rotates to a position with the two magnets aligned, the channel is squeezed by the magnetic force between the two magnets. Through controlling the rotation of the motor shaft to control three magnet pairs, peristaltic pumping could be realized. The operation and control of this type of pumps is much simpler in comparison with the pneumatic ones. However, the physical sizes of the magnets limit the minimization of the pump system and the potential interaction between different magnets may weaken the pumping performance. Likewise, tactile pins of a refreshable Braille display has been used to actuate the peristaltic pump synchronously under the control of a personal

computer [40]. This kind of pump has the advantage of easy construction based on commercially available Braille display and does not need too much manipulation on the disposable elastomer chip. However, the pumping flow rate of the tactile pump is very limited because of the low refreshing frequency and displacement of the tactile pins.

Cam-follower structures have long been used for timing of engine valves. The mechanically determined phase angle makes it easy and stable to control the time sequence of the actuation. Besides, displacement of the follower can be designed in a wide range and the refreshing frequency can be controlled by controlling the rotation of the cams. Cams have been reported for constructing peristaltic pump of microfluidics in serval literatures[46,47]. However, these researches directly used the cam surface rather than the followers to compress the microfluidic channel. The friction between the cam surface and the microfluidic chip surface limited the pumping flow rate and may damage the microfluidic chip.

In this chapter, three cams with different phase angles relative to the camshaft was used to actuate followers for compressing the microfluidic channel to conduct peristaltic pumping of microfluidics. The compressing zone on the microfluidic chip has been modified to improve the performance of the pump. Both experimental observation and theoretical calculation have been conducted to study the pumping performances. This pump provides a simple and efficient way to control microfluidic flow, with great flexibility in controlling the pump flowrate and allowable backpressure.

2.2 Design and fabrication

2.2.1 Operational principle and design

Rotating cams with dwell-rise-dwell-return profile are used to actuate the followers to compress the channel sequentially. The mechanism of the compression process actuated by a single cam is shown in Figure 2.1. A DC motor drives the cam to rotate on a stationary camshaft under a microfluidic channel fabricated with polydimethylsiloxane (PDMS) elastomer. The base cycle area of the cam profile has the minimum radius (r_{min}) and the nose area has the maximum radius (r_{max}) relative to the center of rotation. As shown in Figure 2.1 (a), when the base cycle contact with the follower, the follower stays at the lowest position, and the flow channel is not compressed by the follower. When the cam rotates an angle, the nose area of the cam begins to contact with the follower and produces an “lift” to the follower, thus drives the follower to move straight upward, and therefore press the end face against the PDMS covering membrane to block the microchannel as shown in Figure 2.1b. When the cam continues to rotate, the follower leaves the nose area and gradually returns back to its lowest position. The follower moves continuously in the sequence of dwell-rise-dwell-return to open and close the channel when the cam is driven to rotate continuously. The elastic PDMS covering membrane works as a spring to keep the follower end face contacting with the cam surface at all times and counteract the follower inertia. The minimum radius r_{min} and maximum radius r_{max} of the cam profile are designed to be 4mm and 5mm respectively in this paper, so that the lift of the follower perpendicular to the microfluidic chip plane is 1mm. The rising and returning sections of the cam profile are symmetrically designed based on the

modified sine curve for its lower torque and power demand [48], which is of great significance for reducing the size of the motor for actuating the cam. Meanwhile, the identical rising and returning profile allows the cam to rotate both clockwise and anticlockwise without changing the performance of actuation.

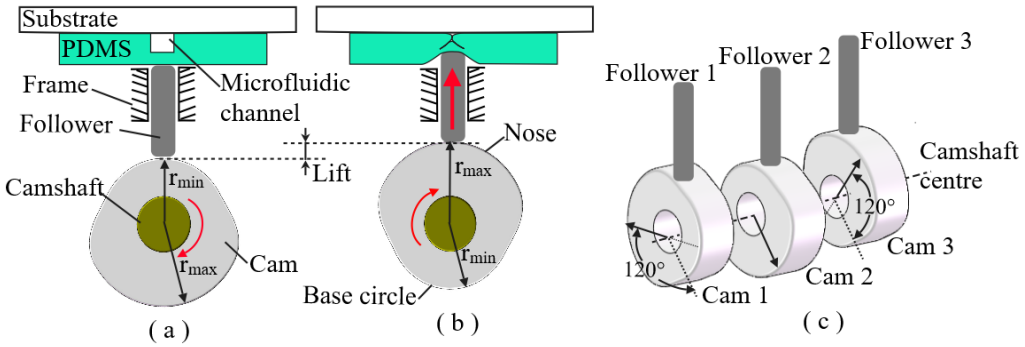

Figure 2.1 Schematic diagram showing the mechanism of cam actuated compression; the channel is open (a) and compressed to be closed (b); three cam-followers constructed peristaltic pump (c)

For each peristaltic pump, a set of three cams is positioned on a camshaft at a 120-degree phase angle difference with each other, as shown in Figure 2.1c. The synchronized displacements of the three followers in each driving cycle are graphically demonstrated in Figure 2.2 a.

Presume the state that the follower dwells at the position of its maximum displacement as ‘1’, and the state when the follower dwells at the lowest position as ‘0’. Correspondingly, the microfluidic channel is closed at state ‘1’ and open at state ’0’. Then the states of the three followers in one working cycle can be expressed as in a sequence of 100-110-010-011-001-101 [49]. Figure 2.2 b shows the schematic diagram of the channel state corresponding to each section of the sequence. By repeating from 100 to 101 states, the

fluid in the channel is pumped to flow right side. The direction of the flow can be easily reversed by change the spinning direction of the cams.

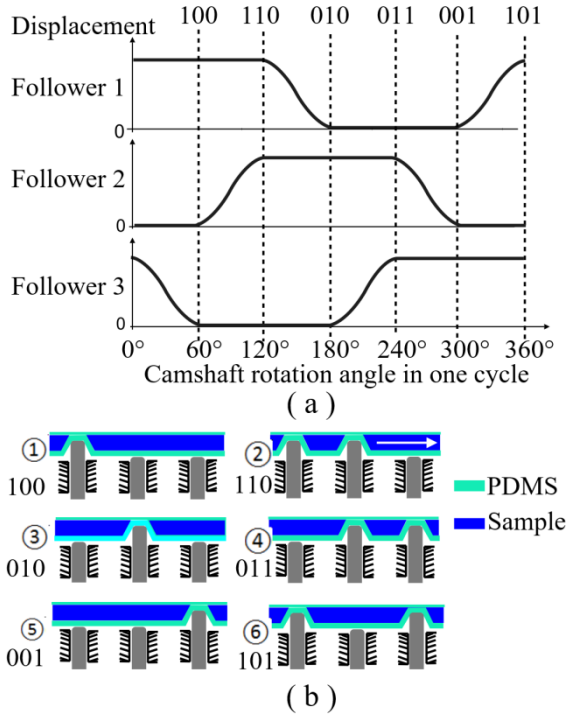

Figure 2.2 (a) Displacement diagram of the three followers for the peristaltic pump; (b) Schematic diagram of the channel states in a working cycle

2.2.2 Fabrication of the cam-follower system and experimental setup

The frame of the system and the cams were manufactured by 3D printing technology using polylactic acid (PLA) as structural material. In order to obtain the 120-degree phase difference between each cam, the three cams were designed and fabricated as a whole unit using 3D printing fabrication. The cam unit was then mounted onto the camshaft. A key was used to mechanically lock the camshaft and cams. A thin layer of polytetrafluoroethylene based dry lubricant (16-TDL, B'laster) was sprayed on the cam surfaces to reduce the friction between the aluminium dowel pins and the PLA cams. Three aluminum dowel pins (McMaster-Carr, Atlanta, GA) with diameter of 3/32 inch served as the cam followers to

squeeze the microfluidic channel under the actuation of the cams. The dowel pins went through the holes of the adjustable-length clevis pins (McMaster-Carr, Atlanta, GA). A pair of steel binder clips was used to fix the microfluidic chip above the dowel pins. The microchannel in the PDMS layer was aligned with the corresponding dowel pins, so the channel could be squeezed by the dowel pins synchronously.

The pump was tested using the setup shown by the photo images in Figure 2.3 a. Three identical cams were fixed on the camshaft with 120-degree phase difference with each other, as shown in the close-up view in Figure 2.3 b. The camshaft was connected to a small DC gear motor (175 rpm, SERVOCITY) through a coupling and was driven to rotate. The motor was powered by 12V power supply and the rotation speed of the motor was regulated through pulse-width modulation (PWM).

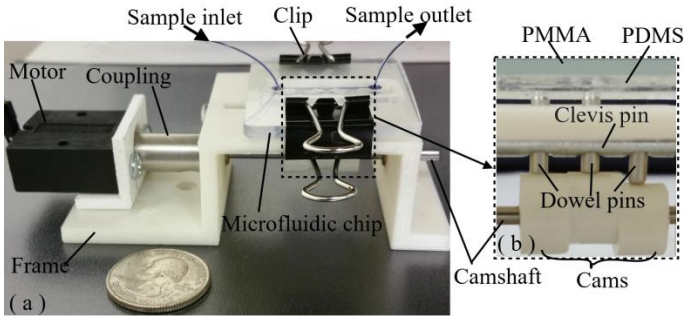

Figure 2.3 (a) Image of the fully assembled setup for pump testing; (b) Close-up view of the cam-follower system (with the clips removed)

2.2.3 Design and fabrication of the microfluidic chip

A microfluidic chip was designed for testing the performances of the pump, as shown in Figure 2.4 a. An inlet reservoir and an outlet reservoir were connected by a microchannel with 150 μm in width and 450 μm in height. Three pins (P1, P2, and P3) are used to compress the microchannel synchronously to pump the liquid sample from the inlet reservoir to the

outlet reservoir. The dotted circles indicate the compressing zone of pin P1, P2 and P3. The channel in the compressing zone of pin P2 was enlarged to be a circular chamber in order to increase the pumping flow rate. Traditionally, the deformation of the channel under compression were enhanced by fabricating the microfluidic channel with round cross section or placing a small ball above the rectangular channel, both of which need extra fabrication process for the microfluidic chip [22,50,51]. In this paper, two cubic chambers were designed and fabricated alongside the channel at each compressing zone to reduce the stiffness of the sidewalls of the micro channel for enhancing the closure of the channel by pin P1 and P3, as shown in Figure 2.4. As the pin squeezes the channel, both the covering membrane and the sidewalls of the channel deform to close the flow channel.

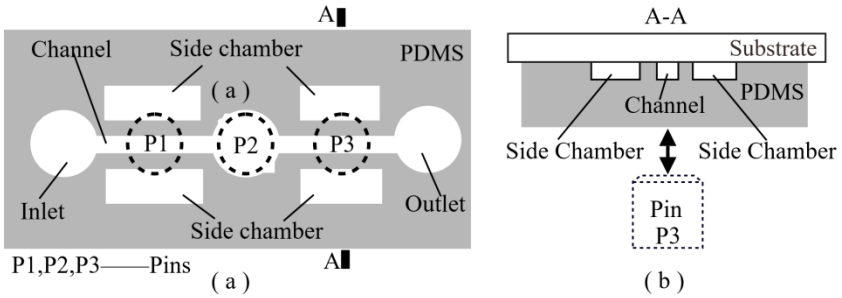

Figure 2.4 (a) Top view for the design of the flow channel and micro chambers for the prototype pump; (b) Cross-section (A-A) view showing the structure of the microfluidic channel

The prototype microfluidic chip was fabricated using a ultraviolet lithography to make master mold and a replica processing [20]. The master mold composed of SU-8 (SU-8 50, Microchem) was first generated on a silicon wafer using UV lithography. Then PDMS (Sylgard 184, Dow-Corning) mixed at a ratio of 1:10 (curing agent to base) was casted onto the SU-8 master mold to form the chip with microfluidic structures. The fabrication flowchart was shown graphically in Figure 2.5. For fabricating the SU-8 master mold, a 4-inch silicon

wafer was cleaned using acetone, isopropyl alcohol and DI water sequentially first, and then dehydrated at 120 ℃ for 10 minutes. After the wafer was cooled to room temperature, a layer of SU-8 with thickness of 450 μm was spin-coated on the cleaned wafer. A UV photolithography was conducted to transfer the pattern on the photomask into cured SU-8 solid structure. Fifteen grams of PDMS mixture was then casted onto the SU-8 master mold and cured at 60 ℃ for 5 h. The PDMS sheet was then peeled off the SU-8 master mold. The molded PDMS structure was then bonded on a 3 mm thick of polymethylmethacrylate (PMMA) plate as the substrate for the microfluidic system. Inlet and outlet holes were punched on the PMMA substrate. The surface of PMMA plate was activated in oxygen plasma for 1 minute and then immersed in 5% (volume /volume) APTES solution at 80 ℃ to form a silylated layer on PMMA surface [21]. After blow-dried, the PMMA plate and the PDMS sheet were treated with oxygen plasma for 36 seconds. They were then bonded together to form the microfluidic chip. The total thickness of the completed PDMS layer was finally measured to be of 2.7 mm.

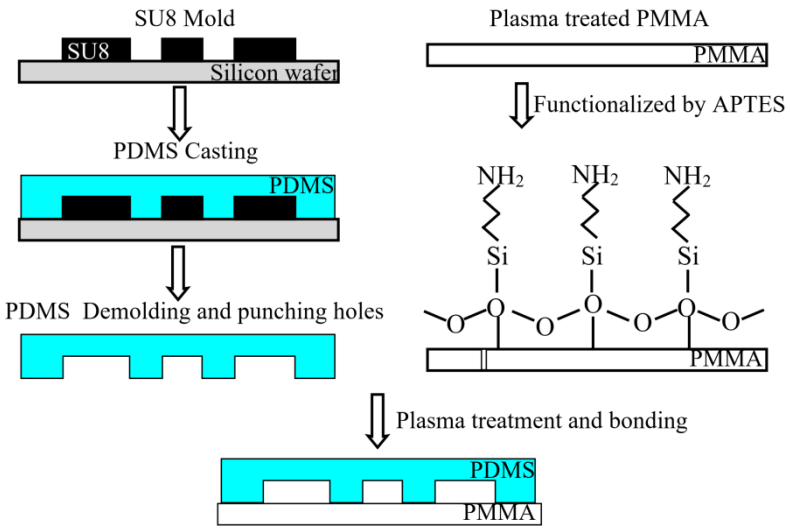

Figure 2.5 Schematic illustration of the fabrication process of the PDMS microfluidic chip

2.3 Experimental results and discussions

Blue ink (KD600X-HB, BCH Technology) was used to test the performance of the pump. Tygon Microbore tube (Cole-Parmer Instrument Company, Illinois; id: 0.25 mm, od: 0.76 mm) was used to connect the inlet of the chip to the ink container and outlet to the following test setup. The pump was self-priming and tolerant of bubbles and particles. The fluid flow direction of the pump can be either from P1 to P3 or reversed, depending on the rotational direction of the motor.

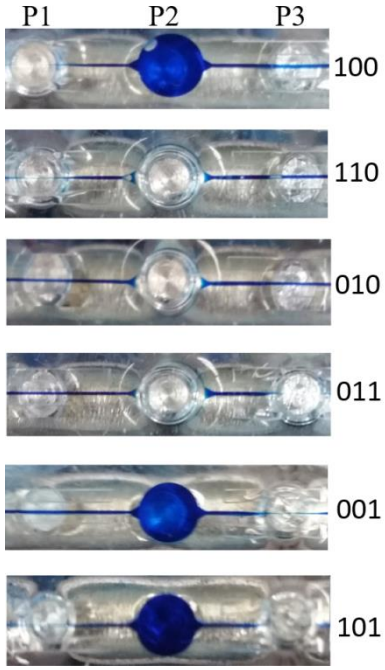

Figure 2.6 Snapshots of the pumping sequence

Figure 2.6 shows the snapshots of the pumping sequences with the flow almost completely cut off by pin P1 and P3. As can be observed from these photos, almost all of the fluids sucked into the middle circle chamber were pumped to the right side except for tiny amount around the edge of the circular chamber. A quick calculation shows that smaller thickness of the side-wall between the channel and side chamber leads to better closure of the

channel. Microfluidic chips with side-wall thickness of 300 μm, 400 μm and 500 μm was tested respectively. For the chips with 300 μm and 400 μm side-wall, the ink was observed leaking into the side chambers in less than 10 min when the driving frequency of the motor was 100 rpm. For the chip with 500 μm side-wall, no leakage has been observed in the side chambers at the compressing zone of pin P1 and P3 after the pump was continuously run for 2 hours at 100 rpm. Therefore microfluidic chip with 500 μm side-wall was used for testing the performance of the pump.

Figure 2.7a shows the setup for testing the pumping flowrate under zero back pressure. Blue ink was injected into the left container which was set at the same level as the microfluidic chip to eliminate the pressure difference caused by gravity. As the pump works, the blue ink was pumped from the left container to the outlet of the chip on the right side. A micro-balance was connected to the outlet of the chip. By weighing the amount of ink from outlet of the microfluidic chip over a given period of time, the average volume flowrate of the pump can be calculated.

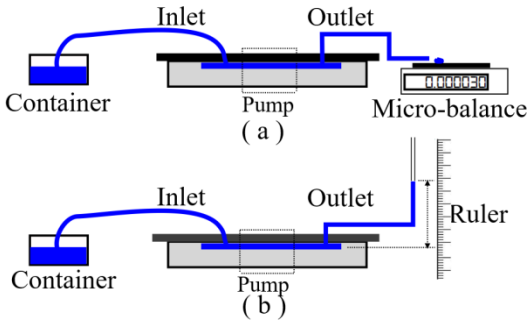

Figure 2.7 Schematic illustration of the setup for flow rate measurement (a) and back pressure measurement (b)

The maximum hydrostatic back-pressures that the pump could work with under different driving speed have been measured using the setup shown in Figure 2.7b. The inlet reservoir

was connected with a container containing blue ink. The container was set on the same level as the chip. The outlet reservoir was connected with a vertical Tygon Microbore tube. As the pump continuously work, the blue ink was pumped from the container into the vertical tube until the ink column in the vertical tube stopped increasing. The height of the column in the vertical tube was measured with a ruler and converted to the backpressure corresponding to the particular driving speed [52]. The Tygon Microbore tube is made of flexible polyvinyl chloride (PVC). The contact angle of water on flexible PVC has been reported to be 87.5 degrees [53]. So the tube shows weak hydrophilic property to the ink solution at room temperature. In the experiment, the capillary rise in a vertical microbore tube was observed to be less than 2 mm which has been neglected when calculating the backpressure.

The pumping flowrates at zero backpressure were firstly tested for different driving frequencies at room temperature. Both the chip fabricated with the aforesaid side chambers (to reduce the effective sidewall stiffness) and the chip without side chambers were tested on the cam-follower pump. The tested results were shown in Figure 2.8. Meanwhile, a simple theoretical analysis of the pumping volume flow rate under zero back-pressure has been conducted. Considering the fact that the volume change of the channel caused by pin P1 and P3 is very small compared with that by pin P2, the fluid volume pumped in one rotation circle can be approximated as the effective volume change (V) of the circular chamber under pin P2.

A simple mathematical model can be used to calculate the pumping flow rate (Q) of the peristaltic pump,

$$Q = fV, \tag{2-1}$$

where *f* is the driving frequency of the motor. For simplicity, the effective volume change (*V*) of the chamber caused by pin P2 can be further approximated as the liquid volume displaced by pin P2. Then the pumping flow rate can be calculated as,

$$Q = \frac{\pi D^2 hn}{4}, \tag{2-2}$$

where *D* is the diameter of pin P2, *h* is the height of the microfluidic channel at the compressing zone of pin P2, and *n* is the rotation speed of the driving motor in revolutions per minute (RPM). The theoretically calculated pumping frequency was also plotted in Figure 2.8. The error bar represents the standard deviation of three measurements at each data point.

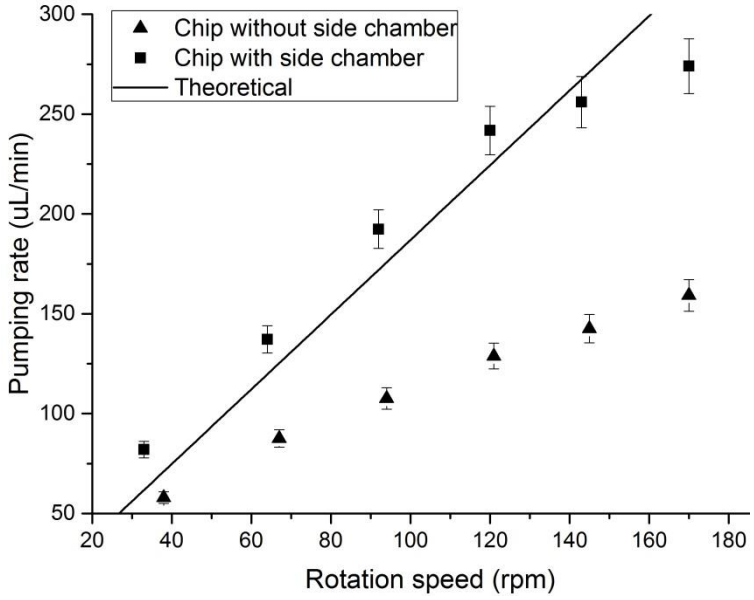

Figure 2.8 Pumping flow rates under zero backpressure as function of rotational speed

From Figure 2.8, it can be observed that the simple mathematical model in Equation

(2-2) provides reasonably accurate predictions of the flow rates. The observed pumping flowrate for the microfluidic chip with side chambers (reduced sidewall thickness) are close to the theoretical ones, especially when the rotation speed is lower than 140 rpm. At lower rotation speed, the measured pumping flow rate is slightly larger than the theoretical calculation. This difference is mainly caused by the simplification in the computation of effective volume change of the circular chamber above pin P2 and the displaced volume by valve 1 and valve 3 which has been neglected in the crude model. When the rotation speed increased over 140 rpm, the observed flowrates deviated more from the theoretical ones. The possible reason for the larger deviation may be that the induced gas bubble at higher driving speed in the circular chamber above pin P2 reduced the actual pumped liquids. Percentage error was calculated for the deviation between the experimental measured flowrates and the theoretical values. The largest error was found to be 32.9% at the driving speed of 33 rpm. The observed pumping flow rate for the microfluidic chip without side chambers is approximately half of the predicted ones from Equation (2-2). This large discrepancy may be caused by the back flow resulted from the incomplete closure of the channel under pin P1 and P2.

From the theoretical calculation in Equation (2-2), the pumping flow rate is proportional to the diameter (D) of pin P2 and the height (h) of the channel above pin P2. Therefore, the pumping flowrate can be customized by changing the diameter (D) of pin P2 together with the change of the channel area above pin P2, or by changing the height (h) of the channel above pin P2.

The maximum backpressure was measured as a function of the driving frequency both for the microfluidic chip with and without side chambers, as shown in Figure 2.9. The error bar represents the standard deviation of three measurements at each data point. The maximum back-pressure of the pump increases with the increase of the rotation speed. In the tested driving speed range, the maximum backpressure for the microfluidic chip with side chambers can reach to 36 kPa at a driving frequency of 156 rpm. The allowable backpressures of the channel without side chambers are much lower than the revised chip, especially when the driving frequency increased over 130 rpm. The increased backpressure for the revised microfluidic chip may attribute to the side chambers which reduced the back flow caused by the incomplete close of the channel.

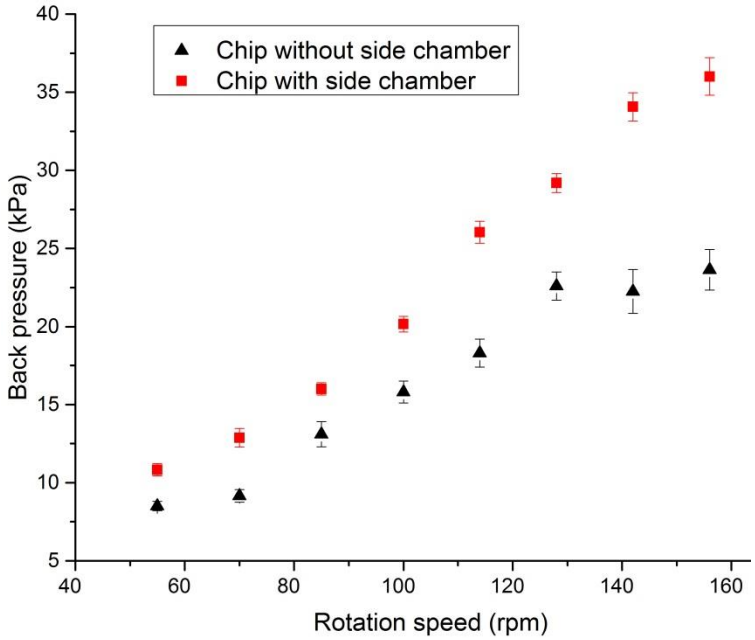

Figure 2.9 Measured maximum back pressure under different rotation speed

Maximum back-pressure is an important parameter for pumps of microfluidic system. In reported literatures, M. Shen et al. actuated a similar PDMS peristaltic pump using three pairs of magnets and realized a maximum backpressure of 6.6 kPa [45]. Yang et al. pneumatically

actuated a PDMS peristaltic pump and the maximum backpressure of the pump was around 85cm-H_2O (~8.5kPa) [42]. The high allowable backpressure of the peristaltic pump in this paper has been an important advantage compared with the state-of-the-art. Besides, it is believable that the revised microfluidic chip design can be used for optimizing the performance of pumps and valves actuated with some other microactuators, such as piezoelectric and electrostatic actuators.

2.4 Conclusions

A micro peristaltic pump has been successfully designed, fabricated, and tested. The pump is actuated using a micro cam-follower system. The microfluidic channel and pumping chambers were fabricated using soft lithography. Three cams with 120-degree phase difference were designed in a combinational cam structure and fabricated using 3-D printing technology. The structure of the pump is simple and can be further minimized and optimized by manufacturing using metallic material. The rotational movement of the combinational cam structure actuates three pins to synchronously compress the PDMS microfluidic channel, therefore pumped the liquid sample in the channel to flow forward. The pumping direction can be reversed easily simply by change the rotational direction of the cam. The experimental results show that this type of the pumps is self-priming and tolerant to air bubbles. Variation of the pumping flow rate could be simply manipulated by controlling the rotation speed of the motor. The function of the pump is independent of the microfluidic chip itself and does not contact with the sample fluid, there is therefore no contamination issue. The experimental results have proved the pump has excellent performances and highly reliable. In addition, the

construction of the pump does not require complex process and the cost can be very low. This concept could be extended to the precise control of multi-pumps with high synchronism. The pump has great potential for applications in microfluidic manipulation for portable point-of-care (POC) systems.

CHAPTER 3. WEDGE ACTUATED NORMALLY OPEN AND NORMALLY CLOSED VALVES FOR CENTRIFUGAL MICROFLUIDIC APPLICATIONS

3.1 Introduction

Centrifugal microfluidic technology has attracted significant attention because of their advantage of the intrinsic pulse-free pumping accompanied with the rotating of the platform [28,54–57]. However, applications of the technology have been limited because of the challenge of integrating suitable valves, which must be both simple and reliable, onto the rotating platform. Various types of valving technologies for centrifugal platforms have been investigated in the past decades. The most commonly used ones are passive valves such as hydrophobic valve [58], capillary valve [59], and siphon valve [60]. These valves are implemented based on the balancing of centrifugal force with surface tension. They offer advantage in reducing the complexity of the system because no external trigger was required except the variation of rotational speed. However, these valves generally require stringent design and manufacturing of the microfluidic channels because of their dependence on the properties of the sample and the fluidic channels, such as the channel geometry and the contact angle between the channel and the sample [61,62]. Besides, most of these valves only work in normally closed state (initially closed and switch to open when triggered) due to the lack of external actuation, and cannot provide physical barrier for handling evaporating reagents.

Active valves, which require external actuations to close or open flow channels, work with low sensitivity to the property of the channels and fluid samples. One important advantage of active valves is the potential use either in normally closed mode or normally

open mode (initially open and switch to closed when triggered). Most of current active valves for centrifugal platform are realized by the phase transition of some blocking substances to switch on or off the channels, such as using hot air or optical illumination to melt paraffin wax, freezing a liquid plug in the channel [63–66]. These innovative phase transition valves offer great potential in promoting the application of centrifugal microfluidics for more complex assays. However, the potential contamination to samples from the melted substance and damage to samples from some unnecessary heating or freezing still limit the application of these valves. The relatively long time required for phase changes and the need to integrate heater or optical source to the centrifugal platform make this type of valves difficult to use. Finally, most of the reported active valves for centrifugal microfluidics are not reversible so that they can only be used for one time. From a literature search, only Park et al. has demonstrated the reversibility of the wax-melting based valves [66].

New valving methods with simple structure and good stability are still keenly needed for Lab-on-CD systems. Pinch valves, which function by compressing the microfluidic channel to block fluid flowing, have been an attractive option because of its widely application for conventional microfluidic control, especially the pneumatic pinch valve pioneered by Quake's group [22]. However, this type of valves needs to be actuated by some external methods, such as pneumatic force, solenoid, screw, and magnetic force [67,68]. One major problem for integrating these pinch valves with the centrifugal platform lies in the difficulty of integrating the traditional actuation and control signal to the rotating platform. When the platform rotates, it is difficult to guarantee stable supply of power or gas pressure to the system. Meanwhile

the centrifugal force hinders the motion of moving parts in some traditional actuators, such as the plunger of the solenoid actuator. In order to promote the application of pinch-valves in centrifugal microfluidics, some actuation methods that are stable and easy to be integrated with the Lab-on-CD system should be explored. We have previously reported a flyball-governor controlled pinch valving system for Lab-on-CD platform [50,51,69]. This type of valves shows good stability and reversibility for liquid control on centrifugal platform. However, it can only function in the normally closed mode, and it is also difficult to reduce the physical size of the flyball governor actuator because of the linkage structure used.

This chapter presents a novel approach to integrate a compact pinch-valving system on the rotating centrifugal platform. The intrinsic centrifugal force of the rotating platform is used to actuate the valve system so that no other external actuation is required for the valves. A sliding wedge with two inclined planes is used to drive the pins to close the microfluidic channel. Through the inclined planes of the wedge and the pins, the horizontal motion of the wedge along the microfluidic chip plane is converted to the vertical motion of the pins for valve actuation. Both the normally closed and normally open valves can be realized with this technology.

3.2 Design and fabrication of the valving system

3.2.1 The operational principle and design

The design of the valving system is schematically demonstrated in Figure 3.1. The system consists of a microfluidic disc (with the microfluidic system) and a wedge-based valving disc. The microfluidic disc and the valving disc are fixed tightly on a rotating shaft,

which is driven by a DC motor. The microfluidic disc includes a rigid polymethyl methacrylate (PMMA) substrate and the microfluidic system made with compressible polydimethylsiloxane (PDMS). The displacement of the pin against the PDMS flow channel helps to compress the PDMS covering membrane to block the fluid flowing in the channel.

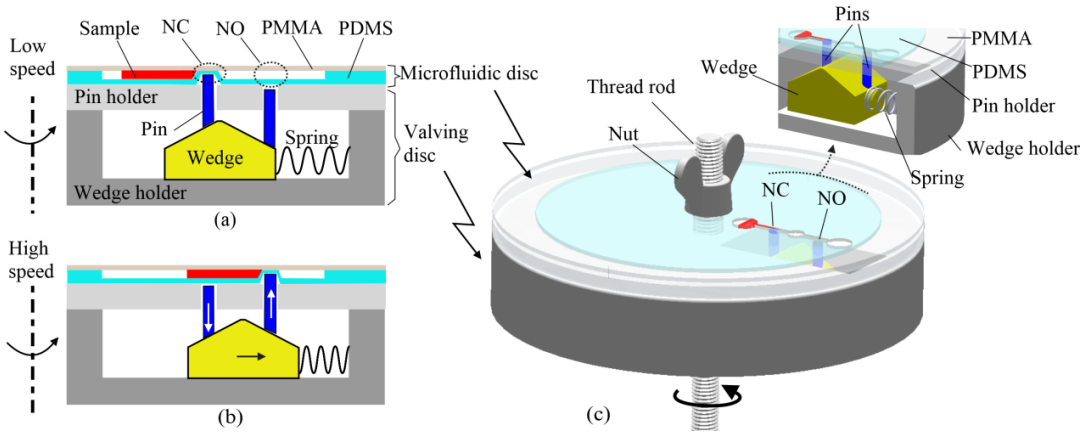

Figure 3.1 Operational principle of the valves on a centrifugal fluidic platform: (a) In stationary or low rotation speed, the normally closed (NC) valve is closed and normally open (NO) valve is open; (b) When the rotation speed is higher than the burst frequency, the NC valve opened and NO valve closed; (c) The assembled centrifugal microfluidic platform. The close-in view shows the schematic design of wedge-spring system

In the valving disc as shown in Figure 3.1, the pins are actuated by a specially designed wedge located inside a slot in the actuation disc. The bottom of each pin has an inclined plane to permit smooth sliding on the top slopes of the wedge. Each wedge has two slopes on its top. One of the slopes is at the inner side close to the centre of the disc and the other is at the outer side close to the edge of the disc. A spring is connected to the outer side of the slot to provide a restoration force. As shown in Figure 3.1a, at low rotation speed, the spring force helps to keep the wedge closer to the rotating centre of the platform. In this condition, the pin on the inner slope stays at high level and it compresses the PDMS layer in the microfluidic

chip above the valving disc. The valve stays closed when the system is stationary or at low speed. It is therefore called the “normally closed” (NC) valve. As the rotation speed of the platform increases, centrifugal force drives the wedge to move outward, and therefore reduce the height of the pin of the normally closed valve. When the rotational speed reaches to a critical value, the valve is opened to permit the fluid sample to pass through as schematically shown in Figure 3.1b. The critical speed is called as the ‘burst frequency’ of the valve.

On the other hand, the pin on the outer slope of the wedge stays at its low position when the platform is stationary or rotates at speed lower than its closing frequency. The microfluidic channel above this pin therefore stays open initially. The valve corresponding to this pin is therefore called a “normally open” (NO) one. When the rotation speed increases to a critical value, the wedge pushes the pin to move upward, compress the covering membrane of flow channel to block the fluid flow, therefore turns off the valve.

In order to test the functionality of this valve design, a prototype microfluidic chip was designed and fabricated. The pattern of the microfluidic chip is graphically shown in Figure 3.2. The chip consists of three valves, with valve 1 and valve 2 as the normally closed ones and used to control the release of liquid samples stored in chamber A and B respectively, while valve 3 is a normally opened valve designed to block the liquid in chamber C when the platform is at high rotation speed. Chamber D is a waste reservoir. The cross sections of the microfluidic channels at the location of the valves are designed to be 800 μm in width and 350 μm in height.

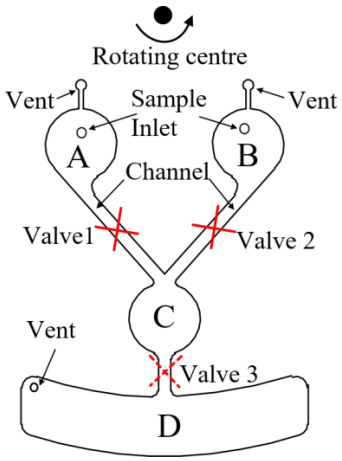

Figure 3.2 Schematic diagram of the microfluidic chip on the rotational platform

3.2.2 Fabrication of microfluidic chip and construction of the prototype system

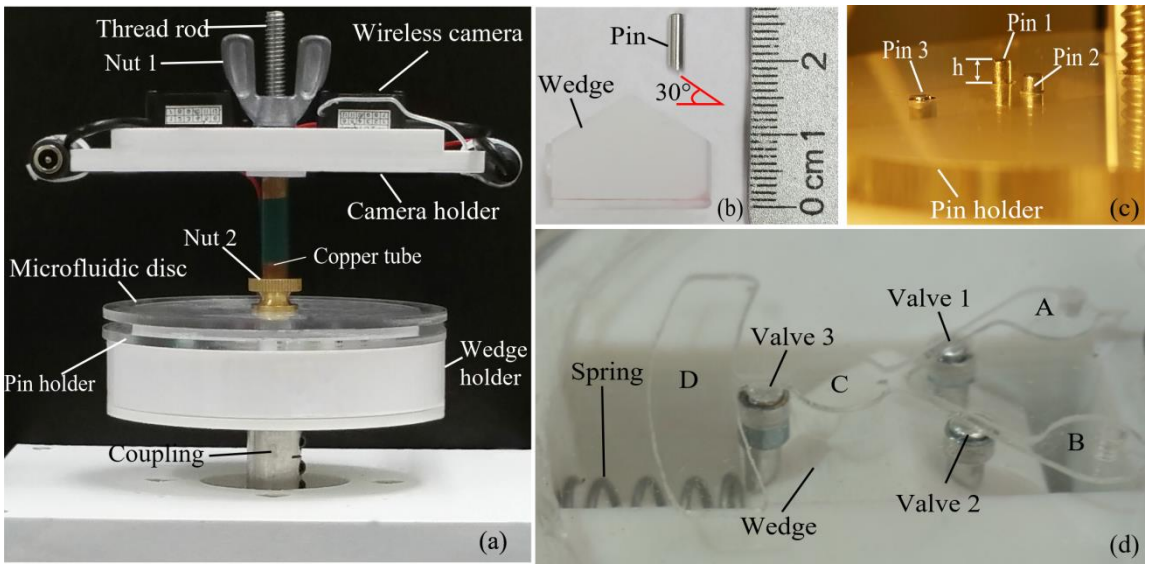

Figure 3.3 Photo images of the prototype centrifugal system:(a) Assembled prototype system; (b) Demonstration of a pin and a wedge; (c) Images of the three installed pins in the pin holder and the initial pin height *h*; (d) Close-up image of the valves

The centrifugal system was fabricated and assembled as shown in Figure 3.3a. A 1/4 inch thread rod was connected to a brushless servo motor (ClearPath, Teknic, Inc.) using a coupling to serve as the rotating shaft of the whole system. The microfluidic disc and the valving disc were fixed together on the shaft using Nut 2. Two wireless sensors were fixed symmetrically on a camera holder mounted on the thread rod with Nut 1. The camera holder synchronously rotated with the centrifugal system so that the cameras could monitor the

motion of the fluids in the microfluidic channels. A copper tube was installed between Nut 2 and the camera holder to adjust the field of view of the cameras. Two 9-Volts batteries were symmetrically installed into the wedge holder to supply power for the cameras when the platform was rotating.

The shell of the wedge, the wedge holder disc (valving disc), and the camera holder were fabricated using 3D printing technology with polylactic acid (PLA) material. Small-sized lead cubes of different masses were filled in the PLA shell of the wedge to adjust the total mass of the wedge. Cylindrical aluminium pin with diameter of 3/32 inch was machined to a certain length with a slope of 30 degree at one of the ends, as shown in Figure 3.3b. The slope surface of the wedge, the pin, and the surface of the slot in the wedge holder were all polished and sprayed with a thin layer of polytetrafluoroethylene based dry lubricant (16-TDL, B'laster) which was typically stable and durable to reduce the friction on the contacting surfaces. After the spring and wedge were installed in the slot of the wedge holder, a 1/8 inch thick pin holder made of PMMA was mounted above the wedge holder. Three through-holes were drilled on the pin holder. Brass spacers with 3/32 inch inner diameter were mounted into the through-holes to achieve the vertical and smooth motion of the pins. Then the pins were installed into the brass spacers. The inclined end of the pins contacted with the corresponding inclined plane of the wedge. The initial pin height (h) is defined as the pin length above the pin holder when the microfluidic disc is not installed, as shown in Figure 3.3c. When the microfluidic disc was installed above the pin holder with the PDMS layer facing the pin holder, the pins in the pin holder push against the PDMS

membrane covering the microfluidic chip, therefore helps to close the flowing fluid in the channel as shown in Figure 3.3d.

The microfluidic chip used for testing the performance of the valves was fabricated using a soft lithography process [20]. As shown in Figure 3.4a, master mold for PDMS casting was first generated on a 4 inch clean silicon wafer using UV photolithography of SU8-50 (Microchem, USA). Then 15g PDMS (Sylgard 184, Dow-Corning) mixed at a ratio of 1:10 (curing agent to base) was casted onto the SU8 mold and degassed in vacuum for 30 min. After cured in oven at 60 ℃ for 5 h, the PDMS replica sheet was peeled off the SU8 master mold and then punched with vent holes and centre holes. A 3 mm thick PMMA disc was used as the substrate for the microfluidic system. In order to form irreversible bonding between the PMDS sheet and the PMMA disc, the surface of PMMA disc was functionalized using 5% (volume/volume) APTES aqueous solution [21]. The surface of PMMA disc was activated in oxygen plasma for 1 min and then immersed in 80 ℃ APTES solution to form a silylated layer on PMMA surface. After blow-dried, the PMMA disc together with the PDMS sheet were treated with oxygen plasma for 36 s. The oxygen plasma treatment resulted in the formation of Si–OH groups on the APTES treated PMMA surface and the PDMS surface. Similar to plasma-based PDMS-PDMS bonding, the two surfaces with Si–OH groups could be irreversibly bonded together after they were brought to contact to form the microfluidic chip disc as shown in Figure 3.4b. The PDMS layer of the chip was finally measured with a total thickness of 2.8 mm.

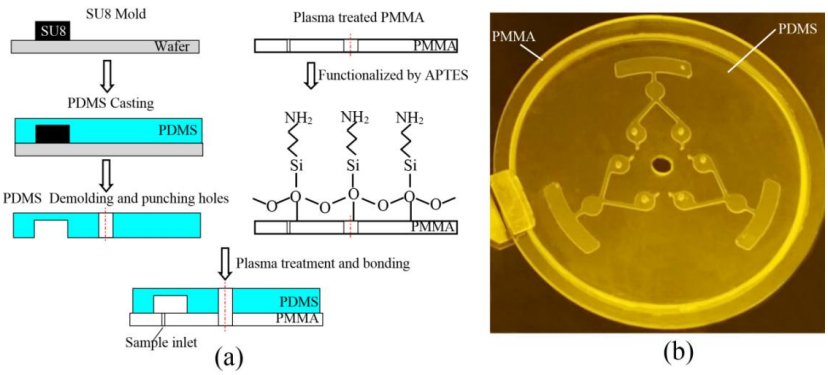

Figure 3.4 (a) Fabrication process of the microfluidic chip and (b) photograph of the prototype microfluidic chip

3.3 Experimental results and analysis

3.3.1 Normally closed valve

The burst frequency of the normally closed valve 1 and valve 2 are tested separately. When a single valve was tested, only the pin for the valve under test was installed on the platform while the other two pins were removed so that they will not affect the tested burst frequency. In order to test valve 1, blue ink (KD600X-HB, BCH Technology) was loaded in reservoir A. As shown in Figure 3.5a, the pin 1 completely closed valve 1 when the rotation speed was under the burst frequency. When the rotation speed of the platform reached the bust frequency, the valve 1 was open within 1 s and the ink in chamber A started to flow into chamber D, as shown in Figure 3.5b. With the rotation speed maintained at the burst frequency, and the ink in reservoir A was completely pumped into chamber D as shown in Figure 3.5c.

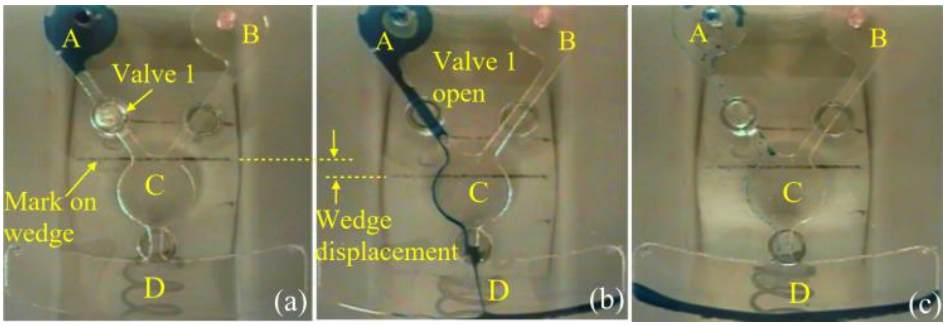

Figure 3.5 Snapshot of the valving process of a normally closed valve: (a) Blue ink was loaded in chamber A; (b) The blue ink in chamber A start to flow into chamber D as the valve 1 was opened; (c) The blue ink in chamber A was completely pumped into chamber D by centrifugal force. The horizontal line across the reaction chamber in the photos is the image of the front edge of the sliding wedge

In Figure 3.5, a horizontal dark line can be observed beneath the reaction chamber. This line is the image of the front edge of the wedge beneath the transparent PDMS fluidic system. The dash lines in the figures demonstrated the displacement of the sliding wedge relative to the fluidic system during the valving process.

An experiment was conducted to check if the pin has successfully moved downward when the normally closed valve was opened. In the experiment, the pin for Valve 1 in Figure 5 was replaced by a bolt with the same end-face size. The bolt was set with an initial height of 0.93 mm and was not free to move either upward or downward during the test. It was observed that the liquid sample was not able to pass through the valve as the rotation speed of the platform was increased up to 4000 rpm, considerably higher than the measured burst frequency (870 rpm) for the Valve 1. The experiment therefore had validated that the pin indeed moved downward to release the fluid sample in the valve operation.

3.3.2 Design for different burst frequencies for the normally closed valves

The equilibrium state of the wedge at burst frequency was studied to obtain a theoretical

estimation of the burst frequency for the normally closed valve. For the sake of simplicity, the pin was assumed to be in complete separation with the PDMS covering membrane at the burst frequency of the valve, as shown in Figure 3.6. The burst frequency of the valves in the manuscript was defined as the rotational speed when the valve is completely open for a normally closed valve. At this moment, the force applied to the PDMS covering membrane by the pin becomes very close to zero and the PDMS membrane is in its equilibrium position under fluid pressure and its elasticity. The effects from the physical properties of the PDMS channel and the liquid sample, such as the Young's modulus of PDMS membrane and the liquid pressure, were therefore not considered in the following analysis. The burst frequency of the valves is therefore only dependent on other mechanical components. The mass of the pin is very small in comparison with the wedge; therefore the reaction force from the pin to the wedge could be neglected for studying the equilibrium of the wedge. In the simplified model, the wedge stays in an equilibrium state under the action of the spring force F_k, the centrifugal force F_c, the friction force f between the wedge and the wedge holder, and the normal force F_N from the wedge holder. The normal force F_N can be approximated to be equal with the weight of the wedge. Because the velocity of the wedge relative to the wedge holder is very small, Coriolis force on the wedge can be neglected. Figure 3.6 shows the free body diagram of the wedge at the burst frequency.

The following equation can then be derived when the wedge of the normally closed vale is in the equilibrium state at its burst frequency,

$$F_c = F_k + f \tag{3-1}$$

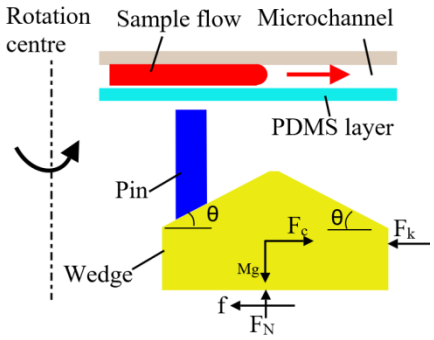

Figure 3.6 The schematic diagram of the pin location and the free body diagram of the wedge

Thus the equation for calculating the burst frequency can be obtained as,

$$M\omega_b^2\left(r_0+\frac{h}{\tan\theta}\right)=\frac{kh}{\tan\theta}+\mu Mg, \qquad (3\text{-}2)$$

where ω_b is the burst frequency of the normally closed valve, μ is the kinetic coefficient of friction between the wedge surface and the slot surface in the wedge holder, h is the initial pin height, θ is the angle of inclined plane of the wedge (θ=30°), r_0 (21.5 mm) is the distance between the centre of the wedge and the rotating centre of the platform when the spring was not compressed. The kinetic coefficient μ, the friction between the wedge surface and the slot surface in the wedge holder, was experimentally measured to be 0.16 using the inclined-plane method. In the measurement, the wedge block was placed on a lubricated inclined plane fabricated with PLA. The angle of the inclined plane was gradually increased at a step of 0.1 degree until the wedge block started to slide downward under slight disturbance as the inclination angle reached a critical value. Then the kinetic coefficient of friction was calculated based on the critical angle of inclination. The spring stiffness k was obtained from the datasheet provided by the vendor (McMaster-Carr). Thus, the burst frequency in revolutions-per-minute (rpm) can be solved as shown in Equation (3-3).

$$\omega_b = \frac{30}{\pi}\sqrt{\frac{\mu M g \tan\theta + kh}{M(r_0 \tan\theta + h)}}, \qquad (3\text{-}3)$$

As can be seen from Equation (3-3), the burst frequency can be adjusted by varying mass M, radius r_0, the initial pin height h, the slope angle of the wedge, and the spring stiffness k.

Both the experimental and simulated results of the burst frequencies for the two normally open valves in the microfluidic chip, the valve 1 and valve 2, as functions of initial pin height, spring stiffness and mass of wedge are plotted for comparison in Figure 3.7, Figure 3.8 and Figure 3.9.

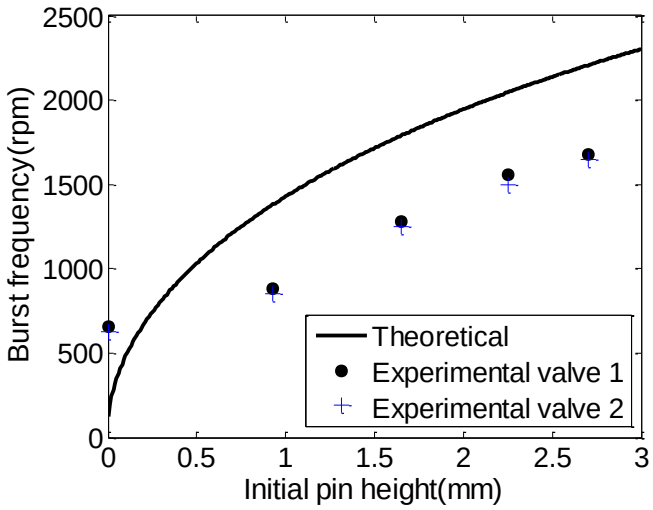

Figure 3.7 Theoretical and experimental results for the burst frequencies of valves as the function of the initial pin height with the mass of the wedge fixed at 13.8 g and the spring stiffness at 4115.5 N/m

In Figure 3.7, when the initial height of the pin was small, the experimentally measured burst frequency was 660 rpm, much higher than the theoretically predicted one using the simplified model of Equation (3-3). The reason is that when the initial height of the pin is set too small, and close to zero, the valve is no longer a pinch-valve, the burst frequency is therefore only determined by the surface tension and Equation (3-3) therefore cannot be used

for calculation. The burst frequency of 660 rpm was determined only by the surface tension. In Figure 3.7, only these burst frequencies higher than 660 rpm were realized under the actuation of the pin-wedge system. Because the valve is a mechanical-pinch valve and the burst frequencies of the prototype valves were all set above 660 rpm (the burst frequency based on surface tension only), all the burst frequencies in Figure 3.7 were found to be higher than 660 rpm.

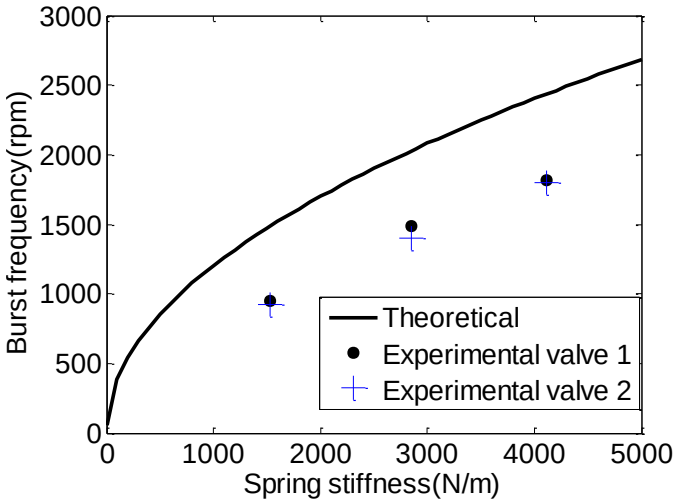

Figure 3.8 Theoretical and experimental results for the burst frequencies of valves 1 and 2 as the function of the spring stiffness, with a wedge mass of 9.7 g and the initial pin height at 2.25 mm

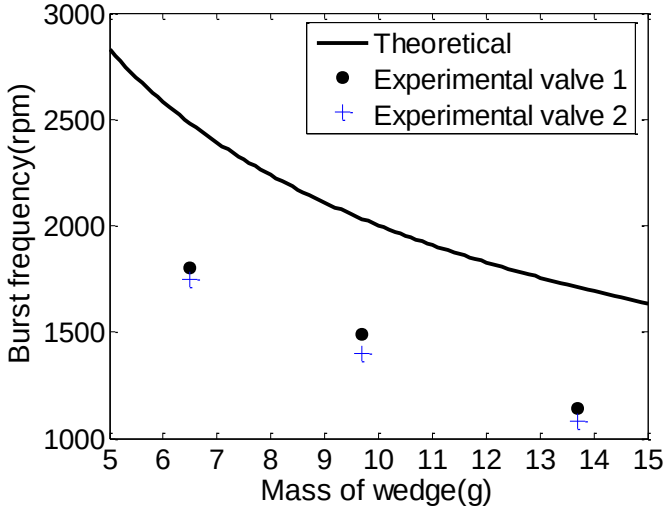

Figure 3.9 Theoretical and experimental results of the burst frequency as the function of the mass of the wedge with the spring stiffness fixed at 2854.6 N/m and the initial height of the pin at 2.25 mm

As can be observed from the results, the experimental burst frequencies of valve 1 and valve 2 are very close to each other and they show the same trend with the theoretical calculation as the initial pin height *h*, the spring stiffness *k* and the wedge mass *M* change. The burst frequencies of the valves increase with the initial pin height and the spring stiffness and decrease as the mass of the wedge increases. As can be observed from the results in Figure 3.7, Figure 3.8 and Figure 3.9, the calculated burst frequencies tend to be higher than experimentally measured ones. One possible reason for the discrepancy is the assumption that the pin has completely separated with the PDMS covering membrane at the burst frequency. In reality, when the fluid started to pass the valve, the pin was still in contact with the PDMS covering membrane and the valve was only partially open. The calculated burst frequencies obtained with this assumption shall therefore be expected to be slightly higher than the measured values.

3.3.3 Experiments of the normally open valves and the microfluidic chip

The experimental results for the microfluidic chip are presented in Figure 3.10. The sequential flowchart for the rotational speed for the platform was graphically demonstrated below the photo images. The weight of the wedge used for the test was 13.8 g. The chamber A and chamber B were loaded with blue ink and red ink respectively, as shown in Figure 3.10a. The initial heights of pin 1 and pin 3, which corresponded to valve1 and valve 3, were set to be at 1.82 mm and -0.36 mm respectively. Pin 2 was removed from the platform so that the valve 2 was controlled only by surface tension. Valve 1 was normally closed and its burst frequency was higher than that of valve 2. Valve 3 was normally open and the

critical rotation frequency for valve 3 to close was between the burst frequency of valve 1 and valve 2 so that the ink in chamber B could pass through valve 3 when released by valve 2 and ink in chamber A could be blocked in chamber C when it was released from chamber A.

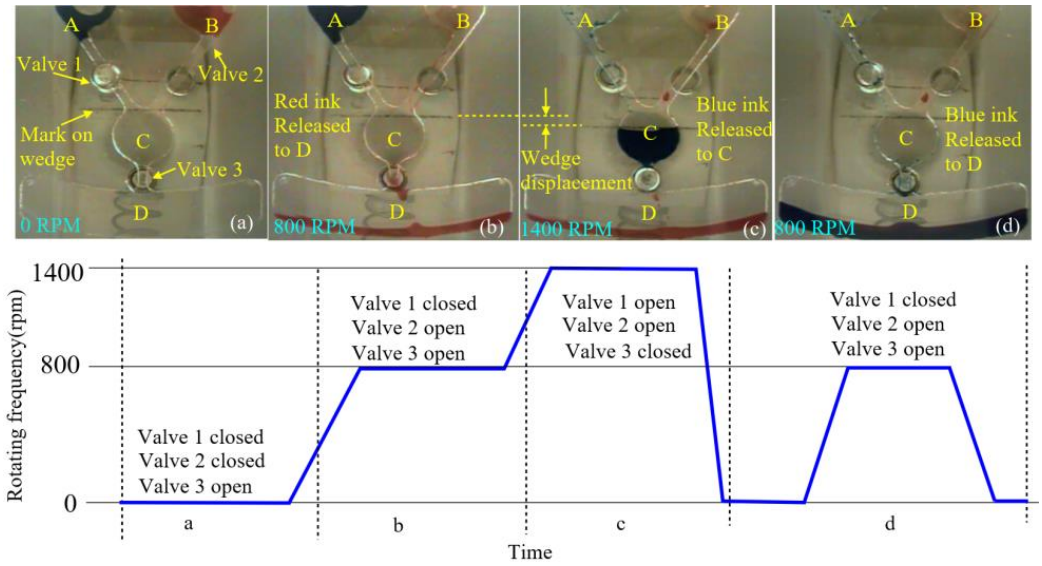

Figure 3.10 Snapshots of the sequential valving process of the microfluidic system and the corresponding rotational speed of the platform

Initially, the blue ink in chamber A and red ink in chamber C was blocked by valve 1 and valve 2. When the rotation speed increased to 800 rpm, valve 2 was opened to release the red ink in chamber B. At this rotation speed, valve 3 was also open, so the red ink directly passed through valve 3, as shown in Figure 3.10b. As the rotation speed of the platform increased to 1400 rpm at an acceleration of 2000 rpm/s, Valve 1 was open and valve 3 was closed. The blue ink in chamber A was released into chamber C and retained in it by the closed valve 3, as shown in Figure 3.10c. The platform was then quickly brought to stop at a deceleration of 2000 rpm/s. Valve 3 was maintained in closed state during the process because of the inertia of the spring-wedge system, therefore the blue ink was still kept in chamber C after the rotation was completely stopped. Then the wedge was gradually pushed

back to its initial location close to the rotation centre by the spring force and valve 3 was opened. The time required for the spring to restore the valve V_3 to open state after the platform returned to the stationary state was measured to be less than 1s. When the platform started to rotate again, the blue ink stored in chamber C passed through valve 3 at 800 rpm, as shown in Figure 3.10d.

The experimental results have proved that both the normally open and normally closed valves can be reversibly realized with excellent reliability. With this valving technology, selectively blocking of sample fluids can be achieved and easily integrated on a Lab-on-CD platform for some complex assays. Samples can be released at lower rotating frequency and blocked at higher frequency through the normally open valve, which otherwise may be difficult to achieve with the existing valving technologies.

It should be noted that because the valving positions on the disc are determined by a given wedge-spring design, a new valving disc needs to be designed for a specific microfluidic disc with different valving positions. With the wedge-actuated valving technology presented in this paper, the microfluidic chip can be replaced and disposable, while the mechanical valving disc consisting of the sliding wedge, pins, and spring, does not have to be replaced. The microfluidic chip itself has very simple structure and were made by replication to reduce the cost. This made it feasible to make the sample-handling microfluidic components disposable, and therefore avoid cleaning requirement for the microfluidic chip. The microfluidic chip may also be fabricated with some other structures and materials, such as the flexible latex membrane structure as reported by other groups to eliminate the concern

of the incompatibility of PDMS with some biology and chemistry assays[70,71]. Additionally, other modules, like the batteries, the control circuits, the optical or electrical detection system, can all be integrated into the valving disc, which makes the whole Lab-on-CD system more compact and integrated.

3.4 Conclusions

By using a sliding wedge to transduce the in-plane centrifugal actuation to the out-of-plane direction and use it to achieve pinch-valving actuation, both normally closed and normally open valves are easily realized for fluidic control on a Lab-on-CD platform. The burst frequency of the valves can be tuned by changing the physical parameters of the actuation mechanism, such as mass of the sliding wedge, spring stiffness, and the initial pin height. The experimental results with prototype valves showed excellent performances and reliability. It can be readily integrated on a centrifugal platform. This valving system is independent of the microfluidic system, and actuation is realized via external contact on the covering membrane of fluidic channels. It therefore brings no contamination to samples in the microfluidic system and can be repeatedly used for disposable microfluidic chips. The valving system has a compact size, and easy to fabricate. Apart from valving, the wedge-pin structure has potential to be used to achieve other microfluidic functions for Lab-on-CD platform, such as mixing and flow switching. Future work will concentrate on applying the valving sytem to some biological assays, like cell screening and detection.

CHAPTER 4. MECHANICALLY PROGRAMMED VALVING TECHNOLOGY AND THE ACTIVE FLOW SWITCHING APPLICATION IN CENTRIFUGAL MICROFLUIDICS

4.1 Introduction

Sequential control of the release of samples is important for integration of multiple analysis steps into microfluidics, especially for biological assays such as DNA analysis [60,72]. For centrifugal microfluidics, the high-speed rotation of centrifugal platform and the limited area of microfluidic disc provide challenge for realizing sequential valving. A wedge actuated valve has been investigated in Chapter 3, but each wedge can only actuate a pair of normally closed valve and normally open valve at the same time [73]. It is still difficult to compactly integrate multiple valves for a single microfluidic system.

In this chapter, a mechanical valving system is made for implementing multiple pinch valves in a small area of the centrifugal microfluidic chip. Spring ball plungers will be used to deform the microfluidic channel to close the valve. The vertical location of these spring ball plungers will be controlled by some grooves on the surface of a valve chip. The valve chip with grooves on the surface was driven to move along the radius of the disc by centrifugal force to change the relative location between the plungers and the grooves. The sequence for opening and closing the valves can be mechanically programmed on the valve chip by designing the location of the grooves. The concept design and the fabrication of the valving system were firstly introduced. The performance of the valves was then theoretically predicted and experimentally tested.

4.2 Materials and methods

4.2.1 Design of the valving system and the microfluidic chip

The detailed design of the valving system is schematically demonstrated in Figure 4.1. A valving chip was built under the microfluidic chip as shown in Figure 4.1a. The microfluidic disc and the valving chip are fixed on the same shaft and driven to rotate together by a DC motor. In this design, the valving actuation is separated from the microfluidic chip. The advantage is the microfluidic chip can be disposable, while the valving chip is a permanent component of the Lab-on-CD instrument. As part of the microchannel, a chamber was designed on the backside of the microfluidic chip. The valving chamber is located above a spring plunger. The vertical location of the spring plunger was controlled by a valving actuation chip with grooves designed on its top surface. A sliding weight is attached to the valving chip and connected with a spring, which provides a balance force to the centrifugal force. The weight is attached to a guide rail and can slide on it. When the rotation speed increases, the centrifugal force increases and drives the weight and the valving chip to slide toward the edge of the rotating disc against the spring force. When the rotation speed decrease, the centrifugal force will decrease and the spring force helps to restore the weight and the valving chip to initial position. As the valving chip moves inside or outside, the grooves on its top helps to drive the spring-plunger to up/down. This helps to convert the horizontal motion of the valving chip and weight to the vertical motion of the spring-plungers. The vertical movement of the spring plungers can then be used to compress the covering membrane of the valving chamber to block the fluid flow.

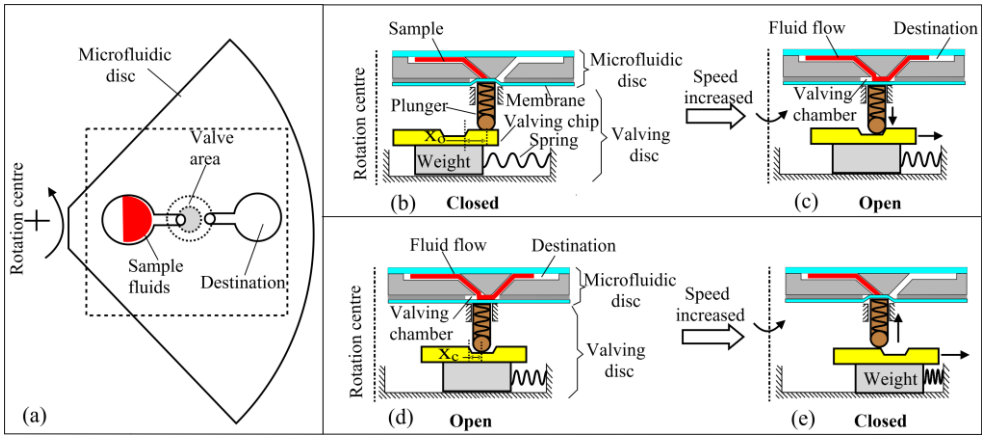

Figure 4.1 Operational principle of the valves on a centrifugal fluidic platform: (a) Top view of one fourth of the microfluidic chip disc; (b-c) Operation of a normally closed valve to open from initial closed state; (c-d) Operation of a normally open valve to close from initial open state

The sequence of the valving action was shown in Figure 4.1(b-d). Each valve requires one particular spring-ball-plunger beneath its valving chamber to block the flow of fluid sample. The vertical location of the plunger can be changed by varying the grooves on the valving chip. The spring plunger has a rotatable ball on its contact point with the upper surface of the valving chip to reduce the friction. When the plunger stays outside of the groove (at higher position), it pushes against the covering membrane of the valve area, causing a deflection of the membrane into the valving chamber to block the fluid flowing through it. On the other hand, when the plunger drops into the groove of the valve chip (lower position), the spring plunger releases the membrane above it to open the valve.

The diagrams in Figure 4.1(b-c) graphically demonstrated the opening operation of a normally closed valve at increased rotation speed. Figure 4.1(d-e) shows the closing operation of a normally open valve at increased rotation speed.

The relative distance between the pin and the edge of the groove when the platform is stationary determines the critical rotation speed, the “burst frequency”, for the valve to open

or close. The distance x_o in Figure 4.1b and x_c in Figure 4.1d respectively shows the distance that the valve chip should move to open or close the valve. Larger initial pin-groove distance means higher "burst speed" is required. Besides, the spring stiffness and the weight under the valving chip could also be tuned to meet the demand of different burst frequencies for valves.

In some biological, chemical and medical assays, sequentially control of multiple valves is needed. For such applications, multiple grooves can be programed onto the surface of the valving chip, with one groove for each valve. With different pin-groove distances selected for individual valves, the burst frequency of each valve can therefore be differentiated. When different control sequence of the valves is required for new application, the valve chip could be easily replaced with a new one with different groove patterns without change of other components in the system.

4.2.2 Construction of the system

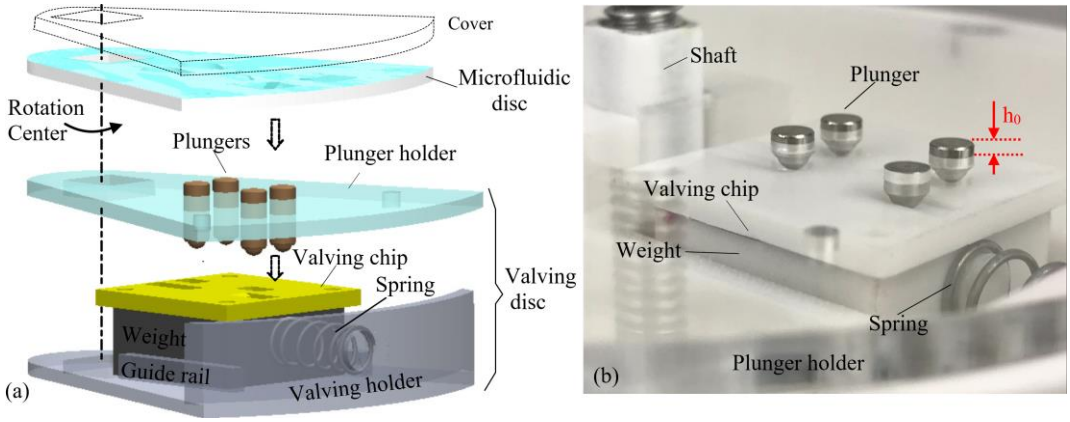

Figure 4.2 (a) The exploded view of the assembly of the system to show the components; (b) image of the assembled valving disc, h_0 is the initial pin height above the plunger holder when microfluidic chip was not mounted

The schematic exploded view of the core structure of the centrifugal microfluidic system, including the valving system and microfluidic system is shown in Figure 4.2a to demonstrate

the assembly details. A slot was fabricated in a disc like valving holder to serve as the guide rail. The weight, spring, and valving chip were installed in the valving holder to form the valving disc. The valving disc was installed under the microfluidic disc. The plunger holder covers the valving disc to support the vertical motion of the plungers. The microfluidic chip was installed tightly above the plunger holder so that the plunger slightly compresses the membrane on the bottom of the microfluidic chip. A rigid cover disc made of PMMA was fixed above the microfluidic chip to prevent the microfluidic chip from deforming when compressed by the pins.

The frame of valving holder, the shell of the wedge and the valve chip were modelled in Solidworks (Dassault Systemes SolidWorks Corp, USA), and fabricated using fused deposition modelling (FDM) printer (Creator Pro, Flash Forge) with polylactic acid (PLA) material. The surface of the slot in the valving holder were all polished and sprayed with a thin layer of polytetrafluoroethylene based dry lubricant (16-TDL, B'laster) which was typically stable and durable to reduce the friction on the contacting surfaces. The fabricated grooves on the valve chip were 0.6 mm in depth and 3 mm in width. Small-sized lead cubes of different masses were filled in the PLA shell to adjust the total mass of the sliding weight. Holes were drilled on a PMMA disc at the valving location to work as the plunger holder. Spring ball plungers with diameter of 3 mm were installed in the holes of the plunger holder and free to move vertically. The initial pin height (h_0) is defined as the pin length above the pin holder when the microfluidic disc is not installed for a normally closed valve, as shown in Figure 4.2b. The value of h_0 determined the compression force from the plunger to the

microfluidic chip in the closed state of the valve. Larger h_0 resulted in larger compression force. A wireless camera was installed above the microfluidic system to monitor the motion of the liquid sample in the microfluidic chip as the platform rotates.

A prototype of microfluidic system was fabricated to test the performance of the valves. For the sake of time and cost, only a portion of the microfluidic disc was fabricated, as shown schematically in Figure 4.3. Microfluidic system was fabricated in a 2 mm thick PLA chip using FDM 3D printer. FDM 3D printing technology enabled the fast prototyping of microfluidic chip with short time and low cost. However, the surface quality of FDM printed suspended structures was poor because of the support material used in the printing process. To avoid this problem, the valving chambers on the bottom of the microfluidic chip were not printed with the microfluidic system in the PLA chip. Instead, the valving chambers were separately fabricated on a 127 μm thick polycarbonate (PC) sheet and then assembled to the 3D printed PLA microfluidic layer. The top and bottom surfaces of the PLA chip was wet sanded using fine grit sandpaper before other components were assembled to it to construct a functional microfluidic chip. The PLA layer and the PC layer was then aligned and bonded together with 100μm thick double-sided pressure-sensitive adhesive (PSA) tape. Finally the top surface of the microfluidic system was sealed using transparent polypropylene adhesive tape (Scotch mailing tape, 3M). The bottom surface of the PC layer was attached with a layer of latex film with thickness of 200 μm to serve as the covering membrane that could be deformed to block the microfluidic channel under the compression of the plunger.

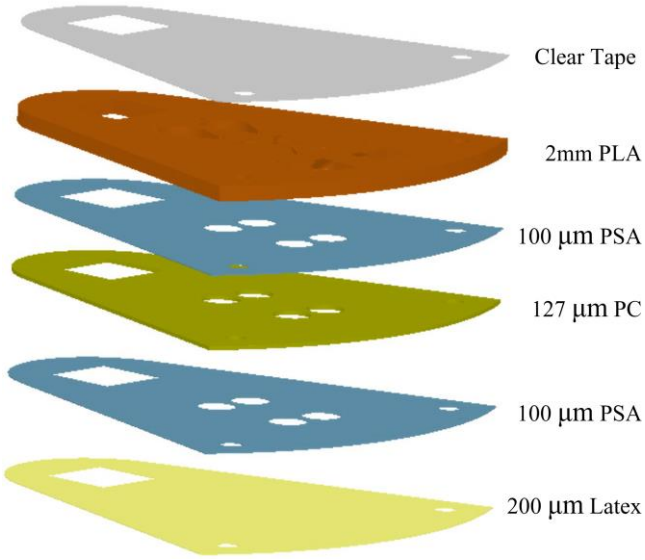

Figure 4.3 The structure of the microfluidic chip

4.3 Experiments and analysis

4.3.1 Single normally closed valve test

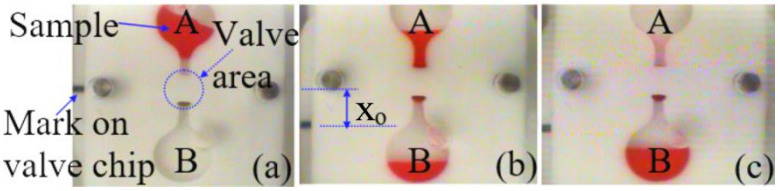

Figure 4.4 Snapshot of the valving process of a single normally closed valve(dotted circle indicates the valving area)：(a) A sample(red ink) was loaded in chamber A; (b) The red ink in chamber A start to flow into chamber B as the valve was opened; (c) The ink in chamber A was completely pumped into chamber B by centrifugal force

Figure 4.4 shows photo images of the operation of a prototype normally closed valve. The flow from the sample-loading chamber A to the destination chamber B was regulated by a normally closed valve. In image Figure 4.4a, red ink was loaded into the sample-loading chamber A when the platform is stationary. The sample fluid could not pass the valve when the rotation speed of the platform is lower than the critical rotation frequency (burst

frequency) of the valve. As rotation speed increased to the burst frequency, red ink passed through the valve and flowed into the destination chamber B. A black line was marked on the valve chip to show the displacement (x_o) of valving chip in the operation, as shown in image b of Figure 4.4.

An experiment was conducted to check if the plunger has successfully moved down into the groove when the normally closed valve was opened. In the experiment, the valving chip with a groove on its surface was replaced using a dummy of the same physical sizes but without grooves on the surface. When the initial pin height was set to be 0.7 mm, the liquid sample was not able to pass through the valve though the rotation speed was increased up to 4000 rpm, considerably higher than the measured burst frequencies for the Valve 1 controlled by a valve chip with grooves on the surface. The experiment therefore had validated that the plunger indeed moved down into the groove to release the fluid sample in the valve operation, and therefore proved the feasibility of using grooves to mechanically program operations of valves.

4.3.2 Design for different burst frequencies for the normally closed valves

The theoretical value of the burst frequency of a normally closed valve can be obtained by analysing the equilibrium state of the wedge in operation. At the burst frequency, the pin moved into the groove area of the valve chip. The restoring force from the latex membrane to the pin, the weight of the pin as well as the friction between the pin and the valve chip are all neglected. So the weight-valve chip assembly stayed at equilibrium in horizontal direction under the spring force F_k, the centrifugal force F_c, and the friction force f between the wedge

and the guide trail, as shown in Figure 4.5, m is the mass of the weight-valve chip assembly. Because the relative velocity of the mass m with respect to the guide trail is very small, Coriolis force on the weight can be neglected.

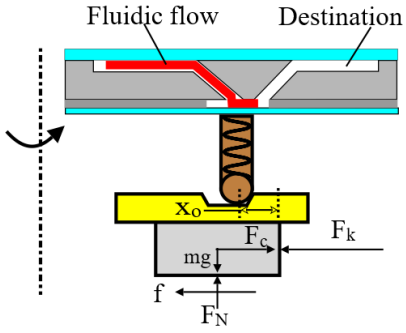

Figure 4.5 The schematic diagram showing the pin location and the weight-valve chip assembly for a normally closed valve at the burst frequency

Thus the equation for calculating the burst frequency can be obtained as,

$$F_c = F_k + f. \tag{4-1}$$

Assuming the normal compressing force from a single pin to the valve chip is $F_{0.}$ There are totally n pins acted on the valve chip, so the normal force (F_N) from the guide trail to the mass can be approximated as,

$$F_N = nF_0 + \text{mg} \ . \tag{4-2}$$

So the burst frequency in rpm with an open displacement of x_0 can be derived as,

$$m\omega^2(x_0 + r_0) = kx_0 + \mu(nF_0 + mg)\,, \tag{4-3}$$

Where ω is the burst frequency of the normally closed valve, x_0 is the initial pin-groove distance of the normally closed valve, r_0 $(22\ mm)$ is the distance between the centre of the weight and the rotating centre of the platform when the spring was not compressed. F_0 was measured to be 2.9 N using a force sensitive resistor (FSR). The kinetic coefficient, μ, of friction between the weight surface and the guide rail, was experimentally measured to be

0.16 using the inclined-plane method [73]. The spring stiffness k was measured based on the principle of Hooke's Law. The springs were loaded in compression to deform with different distances. Each pre-deformation of the spring and the corresponding load were measured using a calliper and digital scale respectively. Then, the spring stiffness can be obtained from the regression analysis in the plot of load as the change of deformation.

The burst frequency in rpm can be calculated from Equation (4-3) as,

$$\omega = \frac{30}{\pi}\sqrt{\frac{kx_0 + \mu(nF_0 + mg)}{m(x_0 + r_0)}} \quad . \qquad (4\text{-}4)$$

As can be seen from Equation (4-4), the burst frequency can be adjusted by varying mass *m*, radius r_0, the initial pin-groove distance x_0, and the spring stiffness *k*.

Both the experimental and simulated results of the burst frequencies for a single normally-closed valve (n=1) in the microfluidic chip as functions of initial pin-groove distance x_0, spring stiffness *k*, and mass of the mass *m* are plotted for comparison in Figure 4.6, Figure 4.7 and Figure 4.8.

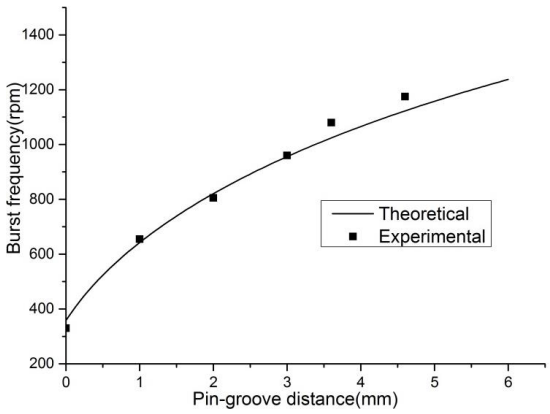

Figure 4.6 Theoretical and experimental results for the burst frequencies of valves as the function of the valving distance. The mass of the wedge was 15.8g and the spring stiffness was 1156.7 N/m

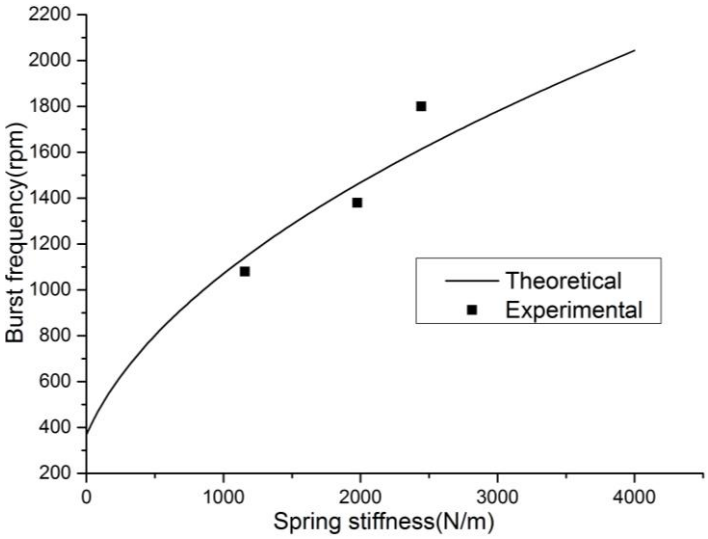

Figure 4.7 Theoretical and experimental results for the burst frequencies of the valve as the function of the spring stiffness, with the mass of 12.7 g and the open distance of 3.6 mm

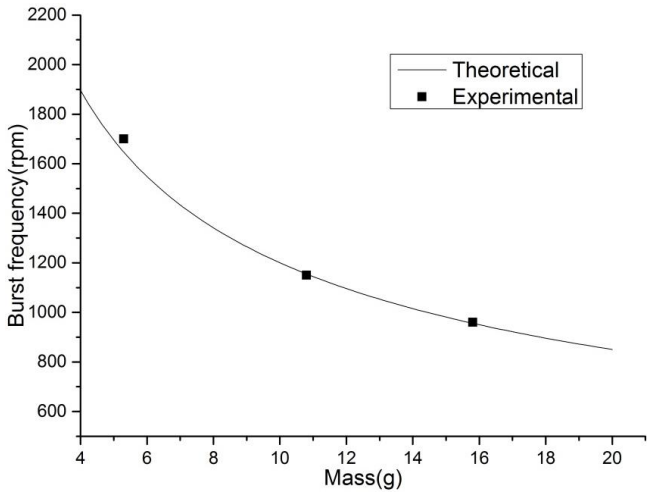

Figure 4.8 Theoretical and experimental results of the burst frequency as the function of the mass m, with the spring stiffness of 1156.7 N/m and the open displacement of 3 mm

As can be observed from the results in Figure 4.6, Figure 4.7 and Figure 4.8, the increases of the initial pin-groove distance and the spring stiffness cause the burst frequency to increase accordingly. Oppositely, the increase of the mass reduces the burst frequency. The effect of the initial pin-groove distance on the burst frequency could be used to design sequentially controlled valves on a single valving chip. The change of mass and spring stiffness can be used to tune the range of the burst frequencies for different applications. By

increasing the spring stiffness or decreasing of the mass, the burst frequencies of the valves can be increased. This may be significant for some bio-assays that are sensitive to centrifugal force, such as blood separation assay.

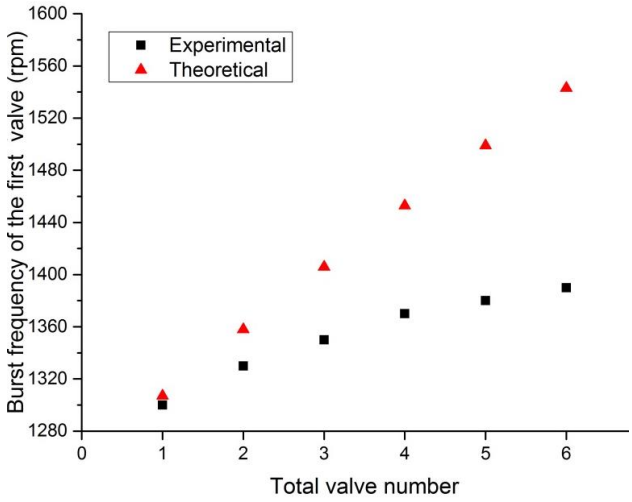

Figure 4.9 The effect of the total number of the valves on the burst frequencies. In these tests, the spring stiffness was 1977.1 N/m, the total weight of the mass and valve chip was 12.7 g, the open distance of the valve chip was 2.7 mm

When multiple valves were implemented, all the plungers for different valves are installed on a single valve chip. From Equation (4-4), the total number of valves, n, affects the calculated burst frequency, because each plunger brings additional compression force to the valving chip, and therefore affecting the friction force applied on the weight. A valve system with 6 normally- closed valves was used to investigate this effect. In these 6 valves, only one valve could turn to open-state in the experiment. No grooves had been fabricated on the valving chip corresponding to the other five valves. The plunger for the openable valve was firstly installed on the platform and the plungers of the other five valves were added into the system one-by-one. The burst frequencies of the openable valve was tested and recorded after each plunger was added to the system, as shown in Figure 4.9.

From Figure 4.9, the burst frequency of the openable valve increased when each following valve was installed. As the addition of each following valve, the simulated burst frequency of the openable valve increased around 50 rpm. However, only a total of around 90 rpm was added to the initial value of the burst frequency in the experiment after all of the other 5 valves were installed. The discrepancy between the theoretical and experimental burst frequency increased as the increase of n. This discrepancy may be caused by the error of the measured value of F_0. From Equation (4-4), the contribution of the error of F_0 to the burst frequency should have increased as the increase of n. As suggested in Equation (4-4), the effect on the burst frequency from the added valves could be further reduced by lubricating the guide rail to reducing the friction coefficient μ.

4.3.3 Implementation of active flow switch

Flow switch is an important unit in centrifugal microfluidics for controlling the flow direction of liquid at intersection of the microfluidic channel in many biological or chemical assays, such as solid phase extraction of DNA from blood [74]. A classic switch for centrifugal microfluidics was constructed based on the Coriolis force on a rotating platform [75]. The change of the rotating direction will change the direction of the Coriolis force on the fluidic sample, so the sample will be directed to different channels. This method needs the switch of the rotating direction and was not effective at low rotation speed [76].The stop of the platform and high rotational frequencies may prematurely trigger other operation units in

the system, such as the siphon and capillary valves, thus add more limitations for disc design [60]. Therefore, a low-speed active switch independent of the rotational direction is

desired for complex centrifugal microfluidic system. Figure 4.10 shows the implementation of flow switch of two outlet channels using four of the proposed valves. V_1, V_2, V_4 are initially closed and V_3 is initially open when the platform stayed stationary. The pin-groove distance for V_1, V_2, V_3, V_4 were designed to be 1 mm, 4 mm, 2 mm, 3 mm respectively. The mass used in the testing is 13 g, and the spring stiffness is 1977.1 N/m.

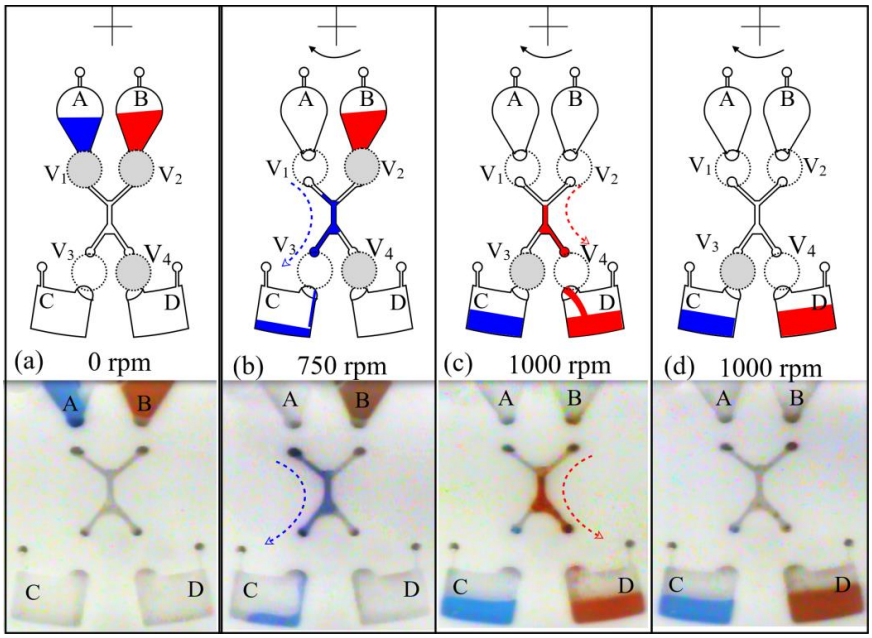

Figure 4.10 Demonstration of flow switch realized with sequential control of multiple valves. The top diagrams (a)-(d) graphically demonstrate the switching process and the images at the bottom are the snapshots of the corresponding steps in the experiment. (a) Position of chambers and valves V1-V4 (shaded area indicated the valve is closed); (b) closed valve V4 forced liquid in chamber A to go to chamber C; (c) valve V3 was closed to force liquid sample flow from chamber B to chamber D; (d) final liquid state

In practical application, there may be multiple middle structures between the source chambers (A, B) and the destination chambers (C, D). Reagents in source chambers (A, B) will be released in to these middle structures sequentially and discharged into different destination chambers (C, D) after being processed. The designed microfluidic system focused on demonstrating the implementation of the flow switch at the intersection to the destination

chambers(C, D). All these middle structures between the sources chambers and destination chambers in the microfluidic system were simplified as a single channel.

Two types of sample (blue ink and red ink) were loaded into the sample chambers A and B respectively to test the performance of the switch. The platform rotated in clockwise direction. When the rotating frequency of the platform increased to 750 rpm, valve V_1 was opened while Valve V_3 stayed open and valve V_4 stayed closed at this frequency. The blue sample in chamber A was pumped into chamber C. From the experiment snap shot, no sample was observed flowing into the right branch. The gas pocket formed between the valve V_4 and the sample flow successfully stopped the sample to flow into the right channel even though the Coriolis force on the liquid sample was pulling the sample to the right side. When the speed continues to increase, valve V_3 was closed and valve V_4 was opened. At 1000 rpm, valve V_2 was opened to release the red sample into chamber D. The entire switching process required no change of the rotation direction and showed the ability to work at relatively low rotation frequency.

4.4 Conclusions

A mechanical valving system was developed for centrifugal microfluidics. It is actuated by the programmed groove pattern and controls the switch sequence of multiple valves simply by manipulation of the rotation speed of the platform. The prototype valves were fabricated using 3D printing technology and tested. The study showed that by changing the physical parameters of the valve system, the burst frequencies of the valves can be adjusted. Flow switch capable of working in constant rotation direction and relatively low rotation

frequency was realized based on sequential control of multiple valves. Compared with other valves reported, the new valving technology was actuated by the intrinsic centrifugal force and requires no external actuation, thus reduced the cost for constructing the system and increased the stability. Additionally, the valving system works independent of the microfluidic system, it could be repeatedly used with no contamination to the fluidic samples. Multiple valves could be realized on the rotating system with compact structures. The valve system could be easily reconfigured for different application by replacing the valve chip with different programmed groove patterns. This valving system shows potential in construction of a flexible centrifugal microfluidic platform for rapid testing of different complex assays with less requirement for tuning the valves for each microfluidic chip, independent of the technology and material used for fabricating the microfluidic chip, and the particular property the fluidic samples.

CHAPTER 5. CENTRIFUGAL MICROFLUIDIC PLATFORM FOR AUTOMATIC COLORIMETRIC URINALYSIS

5.1 Introduction

Point-of-Care diagnostics is attractive in providing rapid disease information for prompt and effective diagnosis and medical treatment to patients. Apart from the significance in dealing with infectious disease outbreaks, Point-of-Care diagnostics has great potential for clinical analysis in developing economies where the existing analytical systems are too expensive to purchase and maintain or too complicated to operate [77]. To reduce the cost and simplify the operation, detection of the disease markers should be achieved with the simplest assays and fewest trained personnel involved if possible.

Colorimetric urinalysis offers an attractive option for point-of-care diagnosing diseases and monitoring medical conditions because of its capability of providing reliable measurements with low cost and high efficiency. Comparing with blood, urine can be noninvasively obtained and easily stored. Colorimetric analysis makes urinalysis cost effective because it requires no expensive equipment to measure or interpret the sensing signals. Qualitative or semi-quantitative colorimetric analysis can be simply conducted by visually inspecting the color change. Some daily electronic devices, such as scanner and smart phone, could be easily used for quantitative colorimetric analysis [78–82]. Currently, colorimetric urinalysis has been used for diagnosing disease such as kidney disorders, diabetes, infections, liver problems, or other metabolic conditions [83]. Many brands of urine reagent strips are commercially available for cost-effective urinalysis. They are commonly used for semi-quantitative determination of urine parameters, such as glucose, protein, nitrites,

PH, specific gravity, ketones, urobilinogen, bilirubin，blood and et al [84]. These dipsticks are portable and cheap for urinalysis. However, careful control of multiple processes are required for conducting urinalysis based on urine reagent strips, including sample loading, read-out time and identification the color change of the pads [85]. Generally, the detection assay was conducted by manually inserting the dipsticks into urine sample and then visually comparing the color change of the strips with standard color chart to identify the parameter value [86]. The manually sample loading process may bring cross-contamination between adjacent pads if sample flows across these pads [87]. Besides, the readout time for different parameters ranges from 30 s to 120 s. For nonprofessionals who want to conduct at-home tests, it is hard to precisely control these readout time after taking the dipstick out of the sample, especially when multiple parameters with the same readout time need to be identified. Additionally, it may be difficult to distinguish the color of one pad with adjacent ones for some parameters. It is therefore difficult to locate the most appropriate standard color to interpret the tested parameters, especially for users with color blindness or under dim environment. All these factors may affect the accuracy of manually conducted strip-based urinalysis.

Microfluidics show advantages in the control of small volume of fluidic sample thus can be used to enhance the colorimetric urinalysis. Colorimetric analysis of urine parameters, such as PH, nitrite, glucose, protein, lactate and uric acid, have been investigated using paper based microfluidics [78,79,82,88]. Paper based microfluidic colorimetric urinalysis automated the distribution of the urine sample. The capillarity of paper automatically pumped urine sample to testing areas where the corresponding reagents were placed. However, the

capillarity actuation of the sample flowing through the testing area of paper-based microfluidics usually increased the non-uniformity of final color change of the testing area, which increased the error of the quantification. Besides, the reported paper based microfluidics for colorimetric urinalysis has difficulties in controlling the sample volume and the read-out time of the color change of these strips because of lacking of valves.

In recent years, microfluidic technology has also been used to improve the commercial strip-based urinalysis process. Smith et.al developed a microfluidic manifold to distribute microliter urine samples to each individual pad of the urinalysis dipstick, thus to eliminate the cross-contamination between adjacent pads [87]. The sample distribution process was accomplished by manually sliding the microfluidic layers. The video of the entire process was captured using a smartphone and analyzed using software to identify the color change of the strips of the dipstick. Their work has promoted the automation of dipstick-based urinalysis, increased the consistency and accuracy of the detection. However, part of the sample distribution process still requires manual work and the acquired high-definition video of the color change process may bring difficulties for storing and analysis.

Centrifugal microfluidics, or Lab-on-CD technology, simplifies the conventional microfluidics by delivering liquid sample using centrifugal force rather than any off-chip pump, thus becomes attractive for portable system for on-site applications.

In this paper, a centrifugal microfluidic platform with a mechanical valving system was used for an automated colorimetric urinalysis. For fast prototyping to prove the feasibility, commercial urinalysis strips were integrated into the microfluidic system for measuring urine

parameters. Urine sample was aliquoted into designed volume and released to react with urinalysis strips in controlled time sequence. The color change of the strips was recorded using smart phone and quantified to find the value of interested parameters in urine sample. A prototype of the system was firstly constructed and tested using red dye. Artificial urine sample was then used for the calibration of the platform.

5.2 Materials and methods

5.2.1 Design of the microfluidic system

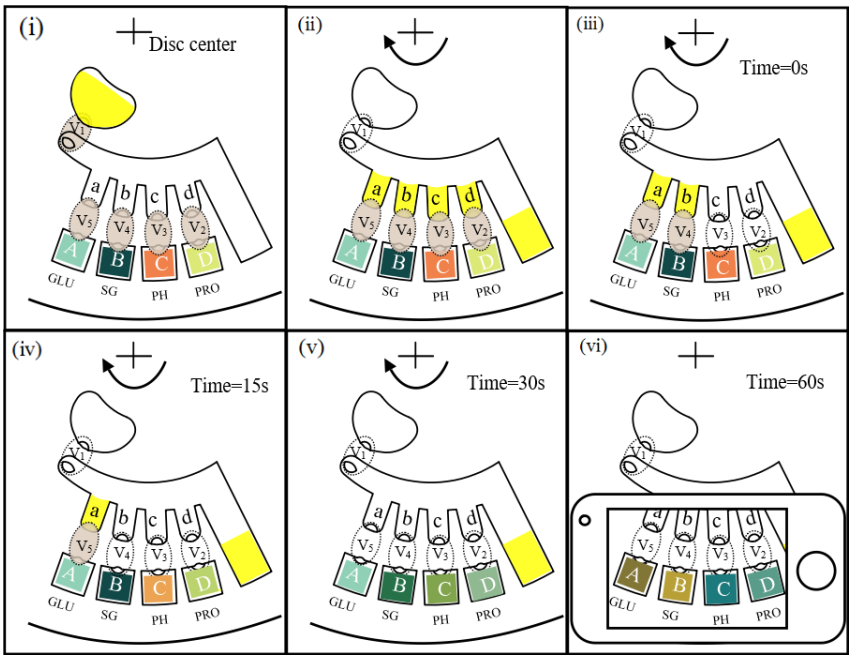

Figure 5.1 Schematic diagrams showing the process flow-chart of the automatic urinalysis using a centrifugal microfluidic platform. V1 to V5 are normally-closed valves, the dotted ovals represent the valving area (shade means the valve is closed). Testing strips for glucose (GLU), specific gravity (SG), PH, and protein (PRO) were sealed in chambers A-D respectively. (i) Urine sample (yellow) is loaded into the sample chamber close to the disc center; (ii) four parts of urine sample are aliquoted from the total sample into chambers a-d; (iii) At time t=0 s, urine samples in chamber c and d are released to chamber C and D respectively; (iv) At time t=15 s, sample in chamber b was released to chamber B; (v) At time t=30 s, sample in chamber A is released to chamber A; (vi) At time t=60 s, a photo image of color strips is taken using a smart phone and the digital image analysis is conducted to find the concentration of analysts

An automatic centrifugal microfluidic platform for urinalysis was designed as shown in Figure 5.1. The measurements of glucose (GLU), specific gravity (SG), PH, and protein (PRO) have been selected to test the functionality of the technology. Microfluidic system was fabricated in a rotational disc mounted on the shaft of a motor. For the purpose of demonstration of the feasibility of the technology, urinalysis strips were used and pre-sealed in the reaction chambers (A-D). According to the specification of the urinalysis strips, the read-out time of the strips for glucose, specific gravity, PH, and protein are 30 s, 45 s, 60 s, and 60 s respectively. Urine sample is loaded into the sample-loading chamber of the microfluidic disc. The sample is then automatically aliquoted into chambers a, b, c, and d. The samples in chambers a-d are then sequentially released into chambers A, B, C, and D respectively to react with the corresponding urinalysis strips. The assay times of the urinalysis for different analysts are controlled by sequential control of these valves. Samples for PH and protein are released to react with their strips first. Then samples for specific gravity and glucose are released after 15 s and 30 s respectively. When all the samples are released into the strip chambers, a high-quality image is taken using a smartphone after 60 s.

The concentration of glucose (GLU), specific gravity (SG), PH, and protein (PRO) in the urine sample are then quantified by comparing the color intensities of the strips with those of calibration curves. There is no cross-contamination between different assay strips because the chambers for the strips are isolated with each other. More importantly, the color change information of the strips is saved in a single high-quality image, which simplified the data acquiring, storing and analyzing process. The valving system could be repeatedly used and

the microfluidic chip can be disposable. The only required operation when conducting the assay are loading urine sample, starting the platform and then taking a picture for analysis with no trained professional required.

5.2.2 Design of the fluidic control system and the microfluidic chip

Figure 5.2 shows the operational principle of centrifugal platform with mechanically programmed valves for metering and sequential releasing urine sample. A valving disc containing all the valving components is installed under the microfluidic disc, as shown in Figure 5.2a. The valve is closed by compressing the deformable covering membrane of the corresponding microfluidic channel using a spring ball plunger installed under the microfluidic chip, as shown in Figure 5.2b. A sliding valving chip with grooves on the surface was used to regulate the vertical location of spring ball plungers. All the plungers initially stay outside the groove, so they compress the cover membranes of the corresponding microfluidic flow channels above them to close the channels. As the valving chip is driven under centrifugal force to a new position when the rotational speed reached a critical value (called the "burst frequency" of the valve), the plunger slides down into the groove and released the compression of the cover membrane above it as shown in Figure 5.2c. The valving chip is mounted on a sliding weight. The relative distance between the plunger-tip and the groove of the valving chip can be varied when the valving chip-weight assembly is driven to slide along a guide rail by the centrifugal force. The plungers have rotatable balls at their ends to reduce the friction forces. The initial distance, x_o, between the plunger tip and the groove determines the burst frequency of the valve. As the rotational speed of the

platform decreases, the centrifugal force drops and the spring helps to restore the valve to its initial state. The valves can therefore be repeatedly used for different microfluidic chips.

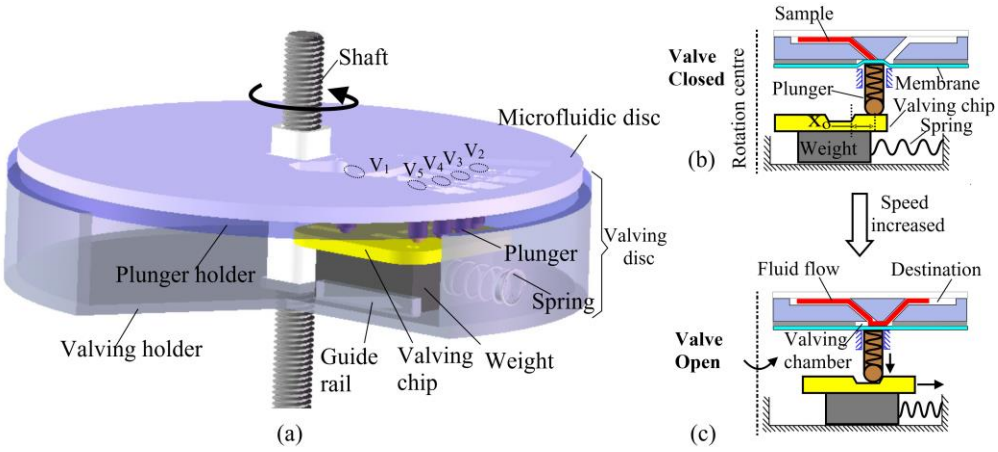

Figure 5.2 (a) Arrangement of the five valves for a centrifugal fluidic chip of urinalysis (the valving holder virtually cut to show the details of the valving system); (b) the initial closed state of the valve when the platform stays stationary or low rotation speed; (c) the valve switches to open at rotation speed higher than burst frequency

For the reported urinalysis device, five valves V_1-V_5 were required and actuated by a single valving chip. The pin-groove distances are 0.5 mm, 3 mm, 3 mm, 3.5 mm, and 4 mm for V_1, V_2, V_3, V_4, V_5 respectively. In operation, valve V_1 opened firstly, followed by valve V_2 and V_3 at the same burst frequency, and finally the V_3 and V_4 are opened successively.

5.2.3 Construction of the Prototype System

Instead of designing multiple fluidic systems for parallel processing of large number of samples, only a portion of the microfluidic disc was fabricated for feasibility study purpose. The fabrication flow-chart for the microfluidic chip was graphically demonstrated in Figure 5.3. Microfluidic system was fabricated in a 2.6 mm thick polylactide (PLA) chip using fused deposition modelling (FDM) 3D printer. The top and bottom surfaces of the PLA chip were wet-sanded using fine grit sandpaper before other components were assembled to it

to construct a functional microfluidic disc. A 127 μm thick polycarbonate (PC) layer with through holes was then aligned and bonded to the 3D printed PLA layer with 100 μm thick double-sided pressure-sensitive adhesive (PSA) tape. After being attached to the PLA microfluidic layer, these through holes in the PC layer formed valving chambers at the valving locations for the plungers to deform into. These valving chambers were then covered with a layer of latex film with thickness of 200 μm. Pads for glucose, specific gravity, PH, and protein were cut from a commercial 10-parameter urinalysis strip (Rapid Response) and mounted into the corresponding destination chambers. Finally the top surface of the microfluidic system was sealed using transparent polypropylene adhesive tape (Scotch mailing tape, 3M). Roller compression was applied on the tape for better sealing to avoid fluid leakage at high rotating speed.

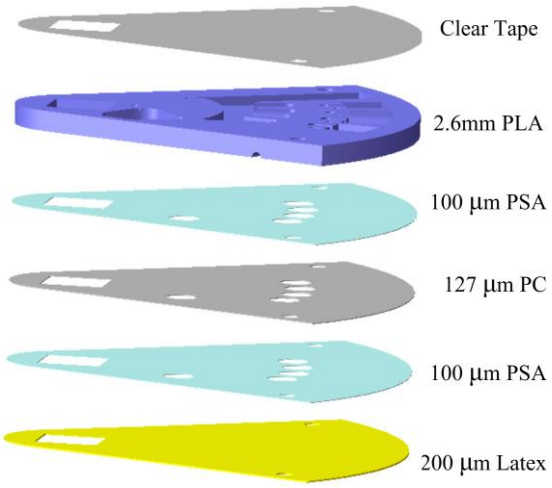

Figure 5.3 The structure of the microfluidic chip

Figure 5.4 (a) shows a photo image of the prototype urinalysis system. Figure 5.4b shows the microfluidic chip installed on a shaft driven by a DC servomotor. The valving system was installed under the microfluidic chip. All of the valving components were

contained in a valving holder. A slot was fabricated in the valving holder to work as the guide rail for the movement of the weight. The holes in the cover of the slots worked as the support for the plungers to move up and down. The weight, the spring, the valving chip, and the plungers were installed in the valve holder sequentially, as shown in image of Figure 5.4c. When the microfluidic chip was fixed above the plungers, the plungers compressed the membrane on the bottom of the microfluidic chip to close the microfluidic channel. A rigid cover disc made of PMMA was mounted above the microfluidic chip to prevent the microfluidic chip from deforming when compressed by the plungers.

The valving holder, the shell of the weight and the valving chip were modelled in Solidworks (Dassault Systemes SolidWorks Corp, USA), and fabricated using fused deposition FDM printer (Creator Pro, Flash Forge) with PLA material. The surface of the slot in the valving holder were all polished and sprayed with a thin layer of polytetrafluoroethylene based dry lubricant (16-TDL, B'laster), which is known to be stable and durable for reducing the friction on the contacting surfaces during relative motion. The fabricated grooves on the valving chip were 0.6 mm in depth and 3 mm in width. Lead cubes were filled in the PLA shell of the weight to adjust the total mass of the weight to be 13 g. The spring stiffness is 1977.1 N/m. Holes were drilled on a PMMA disc at the valving location to work as the plunger holder. Spring ball plungers with diameter of 3 mm were installed in the holes of the plunger holder and free to move vertically.

A smart phone was fixed right above the microfluidic chip. The servomotor was controlled to stop at the same location each time so that the relative location between the

camera of the phone and the microfluidic chip was kept the same. In order to minimize the influence of ambient light, the experiment was conducted in darkroom with constant conditions of illumination.

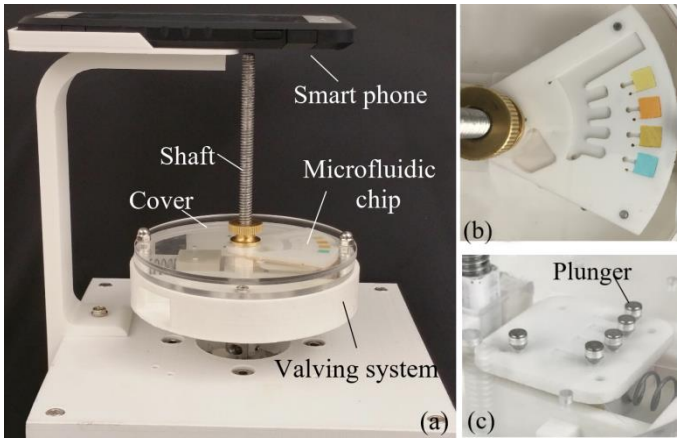

Figure 5.4 (a) Photo image of the setup of the centrifugal platform for urinalysis; (b) photo image of the microfluidic disc; (c) photo imaged showing close-view of the valving system for the centrifugal microfluidic platform

5.3 Experimental results and analysis

5.3.1 Sample aliquot and sequential distribution

In the urinalysis process, the microfluidic system controlled the distribution of the liquid sample in designed volume and designed time sequences. The function of the microfluidic system was firstly tested using red ink, as shown in Figure 5.5. Red ink was loaded in the sample-loading chamber when the platform stayed stationary. A pair of wireless camera was installed above the microfluidic system to monitor the motion of the ink in the chip when the platform was rotating. Then the rotation frequency of the platform increase to 900 rpm, Valve V_1 opened to release the loaded sample into the aliquot chambers a-d. The red ink was aliquoted in the four chambers, each with a volume of 23 μl. After all the excess sample flowed into the waste chamber at the most right side of the microfluidic system, the rotating

frequency increased to 1400 rpm, Valve V_2 and V_3 opened to release the sample in chamber c and d. The timing was initiated at this point. Then at time 15 seconds, the rotation frequency increased to 1500 rpm, valve V_3 opened to release the third sample in chamber b. At time 30 s, the final sample was released at a rotation frequency of 1600 rpm in chamber a. The system realized the designed function of aliquoting and sequential releasing the liquid sample.

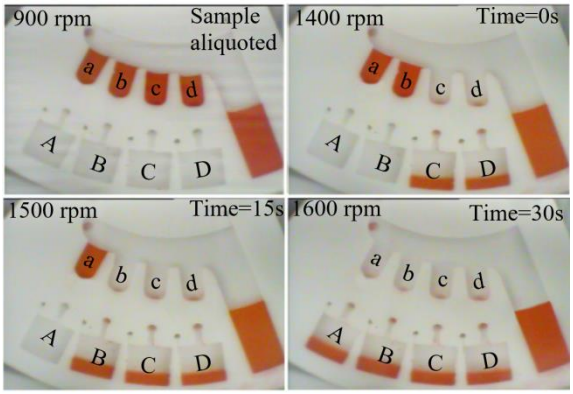

Figure 5.5 Snapshot of the sample aliquot and sequential distribution on the centrifugal microfluidic disc

5.3.2 Implementation of urinalysis and discussions

For calibration and validation of the prototype device, artificial urine sample of known glucose, pH and protein concentrations were prepared. Dextrose (Sigma-Aldrich), sodium chloride (Sigma-Aldrich) and bull serum albumin (BSA) (Sigma-Aldrich) were dissolved into DI water to simulate urine sample. A pH-meter (OAKTON Instruments, model pH/CON 700), calibrated against three standard buffer solutions (pH 4.0, 7.0 and 10.0), was used for measuring the pH of the sample.

The size of the each strip pad is 5 mm (width) by 5mm (length) by 0.8mm (thickness). The size of the destination chamber is designed to be 5.2 mm (width) by 5.2 mm (length). This size design enabled the easy mounting of the strips into the chamber without damaging

the edge and surface of the pad, and at the same time the pads can be tightly fitted in the chambers to withstand actuation of the centrifugal force. The depth of chambers sets the volume limit of urine sample that can be loaded into it. Experiments were conducted for different depths of chambers to find the optimal volume of urine sample for each pad. In order to avoid the leakage of the extra sample loaded into the chamber, vent holes were not fabricated for this test. All the test chambers were completely filled with artificial urine sample. The experimental results are shown in Figure 5.6.

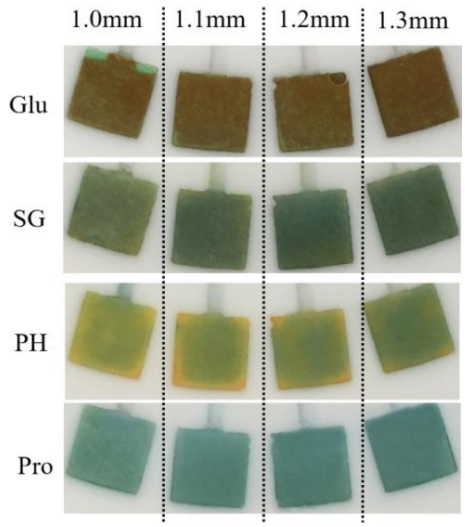

Figure 5.6 Color change of the strip pads under different chamber depth

As can be observed from Figure 5.6, the color change of the strip of PH was most sensitive to the chamber depth. When the chamber depth was less than 1.3 mm, the color at edges of the PH pad did not change as complete as in its central area. At a chamber depth of 1.3 mm, the color change at the edge of PH strip started to be comparable to that in the center of the pad. This depth worked good for all the other three tested parameters. When the depth of chambers was further increased, the uniformity of the color change of the PH pad was slightly improved. However, further increase in chamber depth may have the risk of masking

the color change of the pad when the urine layer above the strip pad is too thick. The optimal depth for the reaction chambers was therefore chosen to be 1.3 mm.

When the chamber depth was designed to be 1.3 mm, the maximum volume of urine sample is found to be at 23 μL. This is the volume to completely fill each destination chamber after analysis pad had been fixed in the chamber. With more than 23 μL, the extra sample fluid may overflow from the chamber into the vent hole of the chamber and cause it to be blocked.

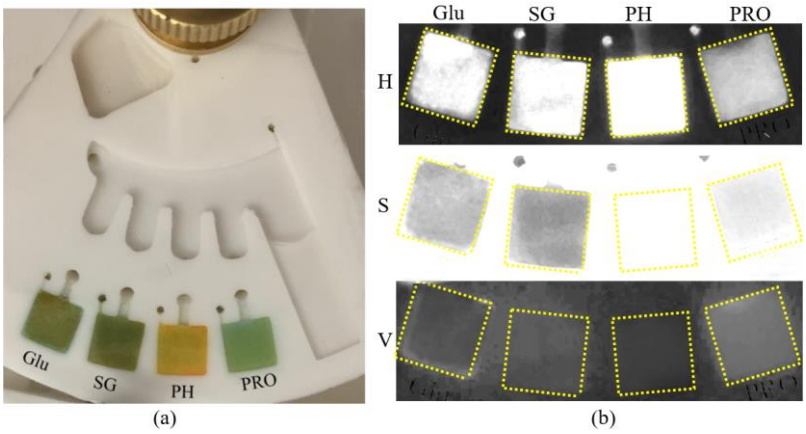

Figure 5.7 (a) Image of the strip pads captured by smartphone at time 60 seconds; (b) photo image of the H, S and V channels

After the controlled artificial urine sample was loaded into the sample-loading chamber, the platform was controlled to rotate at designed speed to complete the aliquot and distribution of fluid sample. The platform was completely stopped after 30 seconds of rotation. After 60 seconds, a picture of the four pads was taken using the smart phone under controlled constant illumination, as shown in the photo image in Figure 5.7a.

We used the ImageJ software to obtain digital color information from the recorded images. The recorded images were firstly converted from the RGB color space to HSV color space and split to H (hue), S (saturation), and V (value) coordinates with the Color Space

Converter plugin of ImageJ prior to the image analysis, as shown in Figure 5.7b. A circular region of interest (ROI, 7860 pixels) was selected around the center of each strip pad for analysis. The values of the H, S, and V coordinates of the recorded image were used to quantify the four urine parameters.

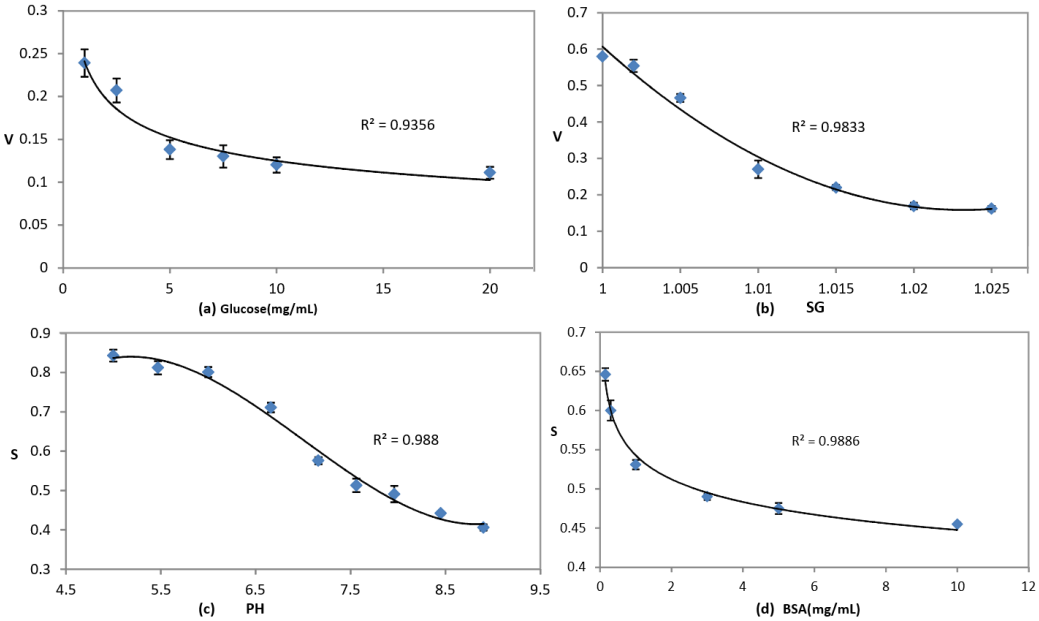

Figure 5.8 Plots of results and fitting curve of the calorimetric urinalysis. The data for glucose (a) and BSA(d) were fitted with power equations; the data for SG (b) were fitted with a quadratic equation ; the data for PH (c) were fitted with a cubic equation

Each experiment was performed three times to find an average and standard deviation for sets of data. As illustrated in Figure 5.8a and Figure 5.8b, the value of V showed good monotony as the change of glucose and specific gravity in the tested range. The glucose in the range of 1 mg/ml to 20 mg/ml and the specific gravity in the range of 1.000 to 1.0025 were measured. As the glucose concentration and the specific gravity value increased, the intensity of the V channel decreased. For glucose, the intensity of V channel changed much faster when the concentration is less than 5 mg/ml. When the value of glucose increased over

5 mg/ml, the change of the intensity of V channel slowed down. The change of V showed good linearity for the change of specific gravity within 1 to 1.010, after that, the change of V slowed down.

For PH and BSA, the change of coordinate S was used to quantify the colorimetric response, as shown in Figure 5.8c and Figure 5.8d. As the PH and BSA increased, the intensity of the S decreased. The tested PH ranges from 5 to 9, which is also the detectable range based on dip-wipe method. When the PH is less than 6 or larger than 8.5, the change of the S was not as sensitive to PH changes. However, the relationship between S channel and PH value became highly linear in the range of 6 to 8.5. With regard to protein (BSA), the intensity of the S decreases as the protein increases. Concentrations in ranges of 0–10 mg/ml were measured, which corresponds to the clinical range [89]. The intensity of S decreases quickly when the concentration of protein is less than 2 mg/ml. The change of S channel became slower when the concentration of protein was larger than 2 mg/ml.

5.4 Conclusions

A calorimetric urinalysis system based on centrifugal microfluidic platform has been successfully demonstrated. The microfluidic platform showed good performance in distributing the urine sample at controlled volume and time sequences. The value of glucose, specific gravity, PH and protein were quantified using artificial urine sample. To test the functionality of the prototype device, a commercial urinalysis strip was cut and inserted into the reaction chambers for detection. The color change of the pads of the urinalysis strip was recorded in a single picture using a smart phone. The obtained color change was converted

into HSV color space for quantifying the urine parameters. V channel shows good monotonic change with the change of glucose and specific gravity. S channel shows relations to the changes in PH and protein. The testing process is fully automated so the users only need to load the sample, start the platform and take a picture of the final color change. The device therefore showed the potential in automated and regulated the urinalysis process at POC. Except for urinalysis, the platform could also be used for other analysis involving in multiple interested parameters, such as blood analysis, drug testing and doping detection.

CHAPTER 6. SUMMARY AND FUTURE WORK

After the fast development in the past decades, the microfluidic technology has demonstrated its great potential in commercial applications though there are still some hurdles to be overcome for broader adoption of the technology. One of these hurdles is that the current control system for microfluidic is still too complex, which makes them not cost-effective and attractive for many commercial uses. In this dissertation, novel controlling methods and components have been investigated to simplify the microfluidic control, and therefore make the technologies more suitable for practical applications.

For conventional microfluidics fabricated on slides, one of the technical difficulties in integration of the entire system is to develop reliable and effective micropump. A compact peristaltic pump for conventional microfluidics was developed. The pump was actuated using a micro-cam array. 3D printing technology was used to fabricate the cam arrays as an integrated component to achieve the desired precision of phase difference between the cams. The proposed pump is compact and requires no complex electronic circuits to regulate the time-sequence. The experimental results have demonstrated good performances and high stability in delivering liquid samples for microfluidic applications.

For centrifugal microfluidics, difficulties in pumping have been overcome by the rotation of the platform. However, valving of sample flows on a rotating platform is still the most significant technical challenges in the control of sample. A novel mechanical valving system actuated by the intrinsic centrifugal force on a sliding wedge has been designed, fabricated, and tested for controlling the sample flow in the microfluidic channel. The

valving system requires no external power, thus reduces the complexity and increased the stability of the centrifugal microfluidic platform.

A wedge actuated valving system for centrifugal microfluidics was then designed, fabricated, and tested. It was further improved for integrating multiple valves in a compact area. The wedge actuated valving system was still actuated by the intrinsic centrifugal force. The grooves on a valve chip were used to control the spring ball plungers to close the microfluidic channel. The application of the new valves on an active flow switch validated its performance in integrating multiple valves in small areas for sequential control.

Finally, a centrifugal microfluidic system with the mechanical valving system in automating the colorimetric urinalysis was designed, fabricated, and tested. The distribution of urine sample was successfully controlled by the valving system. Smart phone based color analysis was used to quantify the urine parameters.

As microfluidics technology evolves quickly, more applications have been demonstrated in laboratory to show its advantages and potentials. User-friendly and cost effective control components are highly demanded for broader adoption of the technologies by industries and market. The pumps and valves demonstrated in this dissertation may help to simplify the control of microfluidic systems for many applications. Future work is still needed to further improve the fabrication technique and device development:

(1) The design and fabrication of the proposed pump and valving system need to be further optimized to make the centrifugal microfluidic platform easier to be used by non-trained users in different fields. The geometric structures could be further minimized using advanced

material and fabrication methods. Utilizing the motion of the sliding weight actuated by centrifugal force to drive hydraulic fluid or gas to actuate pinch valves is another direction worthy further investigation to realize designs requiring higher valve density.

(2) FDM 3D printing technology provided a flexible option to fast prototyping the microfluidic systems. The effect of the printing parameters on the precision and surface quality of the fabricated structures need be studied. The combination of 3D printing technology and traditional photolithography technology can be studied to balance the precision and the fabrication difficulties of some 3D microfluidic system. Additionally, in this dissertation, the bonding of 3D printed layers with latex membrane was realized using double-sided tape. The stability of the tape layer in the microfluidic chip can be negatively impacted by some chemical solvents. The bonding process needs to be further optimized to avoid this problem.

(3) More advanced applications based on the valving and pumping technologies need be investigated. Such applications may include DNA analysis, rare cell screening, chemical sample preparation and et al. The valving chip can also be explored in realizing other microfluidic operations, such as active mixing, inward pumping of the fluidics from the edge to the centre of the disc, so that more complexed assays could be implemented on the centrifugal platform.

REFERENCES

[1] G.M. Whitesides, The origins and the future of microfluidics., Nature. 442 (2006) 368–73.

[2] E.K. Sackmann, A.L. Fulton, D.J. Beebe, The present and future role of microfluidics in biomedical research., Nature. 507 (2014).

[3] P.S. Dittrich, A. Manz, Lab-on-a-chip: microfluidics in drug discovery., Nat. Rev. Drug Discov. 5 (2006) 210–218.

[4] J. Mairhofer, K. Roppert, P. Ertl, Microfluidic systems for pathogen sensing: A review, Sensors (Switzerland). 9 (2009) 4804–4823.

[5] Y. P., E. T., F. E., H. K., N. K., T. M.R., Microfluidic diagnostic technologies for global public health, Nature. 442 (2006) 412–418.

[6] W.G. Lee, Y.G. Kim, B.G. Chung, U. Demirci, A. Khademhosseini, Nano/Microfluidics for diagnosis of infectious diseases in developing countries, Adv Drug Deliv Rev. 62 (2010) 449–457.

[7] Y. Zhang, P. Ozdemir, Microfluidic DNA amplification-A review, Anal. Chim. Acta. 638 (2009) 115–125.

[8] K.M. Horsman, J.M. Bienvenue, K.R. Blasier, J.P. Landers, Forensic DNA analysis on microfluidic devices: a review, J Forensic Sci. 52 (2007) 784–799.

[9] A.A.S. Bhagat, H. Bow, H.W. Hou, S.J. Tan, J. Han, C.T. Lim, Microfluidics for cell separation, Med. Biol. Eng. Comput. 48 (2010) 999–1014.

[10] C. Wyatt Shields IV, C.D. Reyes, G.P. López, Microfluidic cell sorting: a review of the advances in the separation of cells from debulking to rare cell isolation, Lab Chip. 15 (2015) 1230–1249.

[11] P.S. Ashis, K. Sen, Particle separation and sorting in microfluidic devices : a review, (2011).

[12] F.S. Ligler, J.S. Kim, The Microflow Cytometer, 2010.

[13] C. Yi, C.W. Li, S. Ji, M. Yang, Microfluidics technology for manipulation and analysis of biological cells, Anal. Chim. Acta. 560 (2006) 1–23.

[14] H. Yun, K. Kim, W.G. Lee, Cell manipulation in microfluidics, Biofabrication. 5 (2013)

22001.

[15] C.D. Chin, V. Linder, S.K. Sia, Commercialization of microfluidic point-of-care diagnostic devices, Lab Chip. 12 (2012) 2118–2134.

[16] K.S. Elvira, X. i Solvas, R.C. Wootton, A.J. deMello, The past, present and potential for microfluidic reactor technology in chemical synthesis, Nat Chem. 5 (2013) 905–915.

[17] E. Kjeang, Microfluidic fuel cells: A review, J. Power Sources. 186 (2009).

[18] S. Das, V.C. Srivastava, Recent Advances in Fabrication of Photocatalytic Micro-Reactor, Mater. Sci. Forum. 855 (2016) 156–167.

[19] P. Abgrall, A.-M. Gué, Lab-on-chip technologies: making a microfluidic network and coupling it into a complete microsystem—a review, J. Micromechanics Microengineering. 17 (2007) R15–R49.

[20] Y. Xia, G.M. Whitesides, Soft lithography, Annu. Rev. Mater. Sci. 28 (1998) 153–184.

[21] M.E. Vlachopoulou, A. Tserepi, P. Pavli, P. Argitis, M. Sanopoulou, K. Misiakos, A low temperature surface modification assisted method for bonding plastic substrates, J. Micromechanics Microengineering. 19 (2008) 15007.

[22] M.A. Unger, H.P. Chou, T. Thorsen, A. Scherer, S.R. Quake, Monolithic microfabricated valves and pumps by multilayer soft lithography., Science. 288 (2000) 113–116.

[23] Lee, Park, Whitesides, Solvent compatibility of poly (dimethylsiloxane)-based microfluidic devices, Anal. Chem. Dc-. 75 (2003) 6544–6554.

[24] N. Bhattacharjee, A. Urrios, S. Kang, A. Folch, The upcoming 3D-printing revolution in microfluidics, Lab Chip. 16 (2016) 1720–1742.

[25] C.A. Burtis, J.C. Mailen, W.F. Johnson, C.D. Scott, T.O. Tiffany, N.G. Anderson, Development of a miniature fast analyzer., Clin. Chem. 18 (1972) 753–761.

[26] R.M. Rocco, Landmark Papers in Clinical Chemistry, 2006.

[27] M.J. Madou, G.J. Kellogg, LabCD: a centrifuge-based microfluidic platform for diagnostics, BiOS '98 Int. Biomed. Opt. Symp. (1998) 80–93.

[28] O. Strohmeier, M. Keller, F. Schwemmer, S. Zehnle, D. Mark, F. von Stetten, R.

Zengerle, N. Paust, Centrifugal microfluidic platforms: advanced unit operations and applications, Chem. Soc. Rev. 44 (2015) 6187–6229.

[29] J.S.L. Philpot, The use of thin layers in electrophoretic separation, (1939) 38–46.

[30] A. Manz, N. Graber, H.M. Widmer, Miniaturized Total Chemical Analysis Systems: a Novel Concept for Chemical Sensing, Sensors Actuators BI. (1990) 244–248.

[31] K.W. Oh, C.H. Ahn, A review of microvalves, J. Micromechanics Microengineering. 16 (2006) R13–R39.

[32] W. Zeng, I. Jacobi, D.J. Beck, S. Li, H.A. Stone, Characterization of syringe-pump-driven induced pressure fluctuations in elastic microchannels, Lab Chip. 15 (2015) 1110–1115.

[33] Z. Li, S.Y. Mak, A. Sauret, H.C. Shum, Syringe-pump-induced fluctuation in all-aqueous microfluidic system implications for flow rate accuracy., Lab Chip. 14 (2014) 744–749.

[34] W. Wang, C. Gu, K.B. Lynch, J.J. Lu, Z. Zhang, Q. Pu, S. Liu, High-Pressure Open-Channel On-Chip Electroosmotic Pump for Nanoflow High Performance Liquid Chromatography, (2014).

[35] X. Fu, N. Mavrogiannis, S. Doria, Z. Gagnon, Microfluidic pumping,routing and metering by contactless metal-based electro-osmosis, Lab Chip. 15 (2015) 3600–3608.

[36] A. Wixforth, Acoustically Driven Programmable Microfluidics for Biological and Chemical Applications, Ournal Assoc. Lab. Autom. 11 (2006) 399–405.

[37] A.R. Smith, A. Saren, J. Järvinen, K. Ullakko, Characterization of a high-resolution solid-state micropump that can be integrated into microfluidic systems, Microfluid. Nanofluidics. 18 (2015) 1255–1263.

[38] M.B. Romanowsky, A.R. Abate, A. Rotem, C. Holtze, D. a. Weitz, High throughput production of single core double emulsions in a parallelized microfluidic device, Lab Chip. 12 (2012) 802–807.

[39] I. Lee, P. Hong, C. Cho, B. Lee, K. Chun, B. Kim, Four-electrode micropump with peristaltic motion, Sensors Actuators A Phys. 245 (2016) 19–25.

[40] W. Gu, X. Zhu, N. Futai, B.S. Cho, S. Takayama, Computerized microfluidic cell culture using elastomeric channels and Braille displays., Proc. Natl. Acad. Sci. U. S. A. 101 (2004) 15861–15866.

[41] C.H. Chiou, T.Y. Yeh, J.L. Lin, Deformation analysis of a pneumatically-activated polydimethylsiloxane (PDMS) membrane and potential micro-pump applications, Micromachines. 6 (2015) 216–229.

[42] Y.N. Yang, S.K. Hsiung, G.B. Lee, A pneumatic micropump incorporated with a normally closed valve capable of generating a high pumping rate and a high back pressure, 6 (2009) 823–833.

[43] W.H. Grover, M.G. von Muhlen, S.R. Manalis, Teflon films for chemically-inert microfluidic valves and pumps., Lab Chip. 8 (2008) 913–8.

[44] T. Pan, E. Kai, M. Stay, V. Barocas, B. Ziaie, A magnetically driven PDMS peristaltic micropump., Conf. Proc. IEEE Eng. Med. Biol. Soc. 4 (2004) 2639–2642.

[45] M. Shen, L. Dovat, M. a M. Gijs, Magnetic active-valve micropump actuated by a rotating magnetic assembly, Sensors Actuators, B Chem. 154 (2011) 52–58.

[46] X. Zhang, Z. Chen, Y. Huang, A valve-less microfluidic peristaltic pumping method, Biomicrofluidics. 9 (2015) 1–8.

[47] S.G. Darby, M.R. Moore, T. a Friedlander, D.K. Schaffer, R.S. Reiserer, J.P. Wikswo, K.T. Seale, A metering rotary nanopump for microfluidic systems., Lab Chip. 10 (2010) 3218–3226.

[48] H.A. Rothbart, Cam Design Handbook, 2004.

[49] A.G.S.B. Neto, A.M.N. Lima, H. Neff, C.L. Gomes, C. Moreira, Linear peristaltic pump driven by three magnetic actuators: Simulation and experimental results, Conf. Rec. - IEEE Instrum. Meas. Technol. Conf. (2011) 1454–1459.

[50] Z. Cai, J. Xiang, W. Wang, A pinch-valve for centrifugal microfluidic platforms and its application in sequential valving operation and plasma extraction, Sensors Actuators B Chem. 221 (2015) 257–264.

[51] Z. Cai, J. Xiang, B. Zhang, W. Wang, A magnetically actuated valve for centrifugal microfluidic applications, Sensors Actuators B Chem. 206 (2015) 22–29.

[52] J.H. Tsai, L. Lin, A thermal-bubble-actuated micronozzle-diffuser pump, J. Microelectromechanical Syst. 11 (2002) 665–671.

[53] T. Okuda, K. Kurose, W. Nishijima, M. Okada, Separation of Polyvinyl Chloride from Plastic Mixture by Froth Flotation after Surface Modification with Ozone, (2007) 373–377.

[54] D.D. Nolte, Invited review article: Review of centrifugal microfluidic and bio-optical disks, Rev. Sci. Instrum. 80 (2009).

[55] M. Madou, J. Zoval, G. Jia, H. Kido, J. Kim, N. Kim, Lab on a CD, Annu. Rev. Biomed. Eng. 8 (2006) 601–628.

[56] R. Gorkin, J. Park, J. Siegrist, M. Amasia, B.S. Lee, J.-M. Park, J. Kim, H. Kim, M. Madou, Y.-K. Cho, Centrifugal microfluidics for biomedical applications, Lab Chip. 10 (2010) 1758–1773.

[57] J. Ducrée, S. Haeberle, S. Lutz, S. Pausch, F. Von Stetten, R. Zengerle, The centrifugal microfluidic Bio-Disk platform, J. Micromechanics Microengineering. 17 (2007) S103–S115.

[58] P. Andersson, G. Jesson, G. Kylberg, G. Ekstrand, G. Thorsén, Parallel nanoliter microfluidic analysis system, Anal. Chem. 79 (2007) 4022–4030.

[59] M.J. Madou, L.J. Lee, S. Daunert, S. Lai, C.-H. Shih, Design and Fabrication of CD-like Microfuidic Platforms for Diagnostics: Microfuidic Functions, Biomed. Microdevices. 33 (2001) 245–254.

[60] J. Siegrist, R. Gorkin, L. Clime, E. Roy, R. Peytavi, H. Kido, M. Bergeron, T. Veres, M. Madou, Serial siphon valving for centrifugal microfluidic platforms, Microfluid. Nanofluidics. 9 (2010) 55–63.

[61] J.M. Chen, P.-C. Huang, M.-G. Lin, Analysis and experiment of capillary valves for microfluidics on a rotating disk, Microfluid. Nanofluidics. 4 (2008) 427–437.

[62] M. Focke, F. Stumpf, G. Roth, R. Zengerle, F. von Stetten, Centrifugal microfluidic system for primary amplification and secondary real-time PCR, Lab Chip. 10 (2010) 3210–3212.

[63] K. Abi-Samra, R. Hanson, M. Madou, R.A.G. III, Infrared controlled waxes for liquid handling and storage on a CD-microfluidic platform, Lab Chip. 11 (2011) 723–726.

[64] W. Al-Faqheri, F. Ibrahim, T.H.G. Thio, J. Moebius, K. Joseph, H. Arof, M. Madou, Vacuum/Compression valving (VCV) sing parrafin-wax on a centrifugal microfluidic CD platform, PLoS One. 8 (2013) e58523.

[65] M. Amasia, M. Cozzens, M.J. Madou, Centrifugal microfluidic platform for rapid PCR amplification using integrated thermoelectric heating and ice-valving, Sensors Actuators B Chem. 161 (2012) 1191–1197.

[66] J.-M. Park, Y.-K. Cho, B.-S. Lee, J.-G. Lee, C. Ko, Multifunctional microvalves control by optical illumination on nanoheaters and its application in centrifugal microfluidic devices., Lab Chip. 7 (2007) 557–564.

[67] M.G. Bute, A. Sheikh, V.L. Mathe, D. Bodas, R.N. Karekar, S.W. Gosavi, Magnetically controlled valve for flow manipulation in polymer microfluidic devices, Proc. - ISPTS-1, 1st Int. Symp. Phys. Technol. Sensors. (2012) 357–360.

[68] S.E. Hulme, S.S. Shevkoplyas, G.M. Whitesides, Incorporation of prefabricated screw, pneumatic, and solenoid valves into microfluidic devices., Lab Chip. 9 (2009) 79–86.

[69] Z. Cai, J. Xiang, H. Chen, W. Wang, Membrane-based valves and inward-pumping system for centrifugal microfluidic platforms, Sensors Actuators B Chem. 228 (2015) 251–258.

[70] R. Mukhopadhyay, When PDMS isn't the best, Am. Chem. Soc. Anal. Chemestry. (2007) 3249–3253.

[71] M.M. Aeinehvand, F. Ibrahim, S.W. Harun, A. Kazemzadeh, H.A. Rothan, R. Yusof, M. Madou, Reversible thermo-pneumatic valves on centrifugal microfluidic platform, Lab Chip. 15 (2015) 3358–3369.

[72] Y.K. Cho, J.G. Lee, J.M. Park, B.S. Lee, Y. Lee, C. Ko, One-step pathogen specific DNA extraction from whole blood on a centrifugal microfluidic device, TRANSDUCERS EUROSENSORS '07 - 4th Int. Conf. Solid-State Sensors, Actuators Microsystems. (2007) 387–390.

[73] J. Xiang, Z. Cai, Y. Zhang, W. Wang, Wedge Actuated Normally-Open and Normally-Closed Valves for Centrifugal Microfluidic Applications, Sensors Actuators B Chem. 243 (2016) 542–548.

[74] J. Hoffmann, D. Mark, S. Lutz, R. Zengerle, F. von Stetten, Pre-storage of liquid reagents in glass ampoules for DNA extraction on a fully integrated lab-on-a-chip cartridge, Lab Chip. 10 (2010) 1480–1484.

[75] J. Kim, H. Kido, R.H. Rangel, M.J. Madou, Passive flow switching valves on a centrifugal microfluidic platform, Sensors Actuators B Chem. 128 (2008) 613–621.

[76] T. Brenner, T. Glatzel, R. Zengerle, J. Ducrée, Frequency-dependent transversal flow control in centrifugal microfluidics, Lab Chip. 5 (2005) 146–150.

[77] J. Hu, S.Q. Wang, L. Wang, F. Li, B. Pingguan-Murphy, T.J. Lu, F. Xu, Advances in paper-based point-of-care diagnostics, Biosens. Bioelectron. 54 (2014) 585–597.

[78] N. Lopez-Ruiz, V.F. Curto, M.M. Erenas, F. Benito-Lopez, D. Diamond, A.J. Palma, L.F. Capitan-Vallvey, Smartphone-based simultaneous pH and nitrite colorimetric determination for paper microfluidic devices, Anal. Chem. 86 (2014) 9554–9562.

[79] A.W. Martinez, S.T. Phillips, E. Carrilho, S.W.T. Iii, H. Sindi, G.M. Whitesides, Simple Telemedicine for Developing Regions : Camera Phones and Paper-Based Microfluidic Devices for Real-Time , Off-Site Diagnosis, 80 (2008) 3699–3707.

[80] A.K. Yetisen, J.L. Martinez-Hurtado, A. Garcia-Melendrez, F. Da Cruz Vasconcellos, C.R. Lowe, A smartphone algorithm with inter-phone repeatability for the analysis of colorimetric tests, Sensors Actuators, B Chem. 196 (2014) 156–160.

[81] L. Shen, J.A. Hagen, I. Papautsky, Point-of-care colorimetric detection with a smartphone, Lab Chip. 12 (2012) 4240–4243.

[82] D. Sechi, B. Greer, J. Johnson, N. Hashemi, Three-Dimensional Paper-Based Micro fl uidic Device for Assays of Protein and Glucose in Urine, (2013) 16–20.

[83] J.A. Simerville, W.C. Maxted, J.J. Pahira, Urinalysis: A comprehensive review, Am. Fam. Physician. 71 (2005) 1153–1162.

[84] D. Kutter, The urine test strip of the future, Clin. Chim. Acta. 297 (2000) 297–304.

[85] K. Bonewit-West, S. Hunt, E. Applegate, Today’s Medical Assistant: Clinical and Administrative Procedures, Elsevier Health Sciences, 2016.

[86] http://www.rapidtest.com/pdf/URS%201-11(%2006-11-2013).pdf.

[87] G.T. Smith, N. Dwork, S.A. Khan, M. Millet, K. Magar, M. Javanmard, A.K. Ellerbee Bowden, Robust dipstick urinalysis using a low-cost, micro-volume slipping manifold and mobile phone platform, Lab Chip. 58 (2016) 951–954.

[88] W. Dungchai, O. Chailapakul, C.S. Henry, Use of multiple colorimetric indicators for paper-based microfluidic devices, Anal. Chim. Acta. 674 (2010) 227–233.

[89] J.M. William, K.B. Stephan, Clinical Biochemistry: Metabolic and Clinical Aspects, Churchill Livingston, New York. (1995).

VITA

Jiwen Xiang was born in Enshi, Hubei Province, China. He received his bachelor's degree from Department of Mechanical Engineering at Central South University of China in 2010. Then he finished his master's research work at State Key Laboratory of High Performance Complex Manufacturing, a research institute of Central South University, in 2013. He joined Dr. Wanjun Wang's research group of MEMS at Louisiana State University in 2013. His main research interests include mechanical system, MEMS, sensors and actuators.